Non-Nuclear WldS Determines Its Neuroprotective Efficacy for Axons and Synapses In Vivo

Cellular/Molecular

Non-Nuclear Wld^S Determines Its Neuroprotective Efficacy for Axons and Synapses *In Vivo*

Bogdan Beirowski,[1] Elisabetta Babetto,[1] Jon Gilley,[1] Francesca Mazzola,[2] Laura Conforti,[1] Lucie Janeckova,[1] Giulio Magni,[2] Richard R. Ribchester,[3] and Michael P. Coleman[1]

[1]Laboratory of Molecular Signalling, The Babraham Institute, Cambridge CB22 3AT, United Kingdom, [2]Institute of Biochemical Biotechnologies, University of Ancona, Via Ranieri, 60131 Ancona, Italy, and [3]Centre for Neuroscience Research, University of Edinburgh, Edinburgh EH8 9JZ, United Kingdom

Axon degeneration contributes widely to neurodegenerative disease but its regulation is poorly understood. The Wallerian degeneration slow (Wld^S) protein protects axons dose-dependently in many circumstances but is paradoxically abundant in nuclei. To test the hypothesis that Wld^S acts within nuclei *in vivo*, we redistributed it from nucleus to cytoplasm in transgenic mice. Surprisingly, instead of weakening the phenotype as expected, extranuclear Wld^S significantly enhanced structural and functional preservation of transected distal axons and their synapses. In contrast to native Wld^S mutants, distal axon stumps remained continuous and ultrastructurally intact up to 7 weeks after injury and motor nerve terminals were robustly preserved even in older mice, remaining functional for 6 d. Moreover, we detect extranuclear Wld^S for the first time *in vivo*, and higher axoplasmic levels in transgenic mice with Wld^S redistribution. Cytoplasmic Wld^S fractionated predominantly with mitochondria and microsomes. We conclude that Wld^S can act in one or more non-nuclear compartments to protect axons and synapses, and that molecular changes can enhance its therapeutic potential.

Key words: **axon degeneration; Wallerian degeneration; neurodegeneration; slow Wallerian degeneration gene; neuroprotection; neuromuscular junction**

Introduction

Axon degeneration occurs in many neurodegenerative diseases and often precedes neuronal cell body death (Raff et al., 2002; Coleman, 2005; Saxena and Caroni, 2007). Wallerian degeneration, a classical experimental model for axon degeneration, is a rapid sequence of events in distal axons after a period of separation from the cell body (Waller, 1850; Beirowski et al., 2005). It is substantially delayed by the *Wld^S* gene in mice (Mack et al., 2001), rats (Adalbert et al., 2005), and *Drosophila* (Hoopfer et al., 2006; MacDonald et al., 2006). Wld^S is an in-frame fusion protein arising from an 85-kb tandem triplication that does not alter expression of the two parent proteins (Coleman et al., 1998; Conforti et al., 2000; Mack et al., 2001). It comprises the N-terminal 70 aa of multiubiquitination factor Ube4b (N70-Ube4b), the complete sequence of Nmnat1, a key enzyme of nicotinamide adenine dinucleotide (NAD^+) biosynthesis, and a short joining sequence of 18 aa with no known function.

The *Wld^S* gene delays axon degeneration in mouse models of several neurodegenerative disorders, suggesting a molecular similarity between processes regulating Wallerian degeneration and degeneration in some axonopathies (Coleman, 2005; Beirowski et al., 2009). This further indicates the need to dissect the molecular mechanisms of Wld^S.

Previous studies addressing which Wld^S domains are responsible for neuroprotection illustrate the importance of *in vivo* experiments. Whereas NAD^+ overproduction by heavily overexpressed Nmnat isoforms confers axon protection in neuronal explant cultures and, to some extent, in *Drosophila* (Araki et al., 2004; Wang et al., 2005; MacDonald et al., 2006; Sasaki et al., 2006), overexpression of Nmnat1 in transgenic mice at levels similar to Wld^S provides no detectable axon protection (Conforti et al., 2007). Thus, Wld^S and NAD^+ overproduction by Nmnat1 are not interchangeable, and the full axoprotective effect *in vivo* and *in vitro* requires more N-terminal sequences of Wld^S.

A key question about the Wld^S mechanism surrounds the subcellular site of its action (Fainzilber and Twiss, 2006). *In vivo* studies have consistently detected Wld^S only in the nucleus (Mack et al., 2001; Samsam et al., 2003; Sajadi et al., 2004; Wilbrey et al., 2008), suggesting that Wld^S confers its axonal effect indirectly by putative nuclear mechanisms (Araki et al., 2004; Gillingwater et al., 2006; Simonin et al., 2007a). However, the complete absence of Wld^S in other cellular compartments could not be proven experimentally owing to detection limits and there are precedents for proteins acting in a subcellular compartment where they are barely detectable (Hamilton et al., 2001). Interestingly, some indirect, *in vitro* evidence suggests bioenergetic or other axonal roles for Wld^S and its putative mediators (Wang et al., 2005; Yang et al., 2007b) compatible with cytoplasmic and axonal Wld^S presence.

Received Aug. 11, 2008; revised Nov. 8, 2008; accepted Dec. 4, 2008.

This work was supported by the Biotechnology and Biological Sciences Research Council and the German Federal Ministry of Education and Research (BMBF-LPD 9901/8-128). R.R.R. held a Royal Society of Edinburgh/Scottish Executive Support Research Fellowship during the conduct of this study. We are grateful to the staff of the Babraham Institute animal facilities for excellent technical assistance with mouse breeding and to Dr. Simon Walker (Babraham Institute) for assistance with confocal microscopy.

Correspondence should be addressed to Dr. Michael P. Coleman, Laboratory of Molecular Signalling, The Babraham Institute, Babraham Research Campus, Babraham, Cambridge CB22 3AT, UK. E-mail: michael.coleman@bbsrc.ac.uk.

DOI:10.1523/JNEUROSCI.3814-08.2009

 0270-6474/09/290653-16$15.00/0

To elucidate the subcellular locus of Wld^S action *in vivo*, we generated transgenic mouse lines with reduced nuclear targeting and cytoplasmic redistribution of Wld^S. These mice showed surprisingly strong protection of axons and synapses suggesting cytoplasmic Wld^S protected them more effectively for equivalent expression levels. We also show Wld^S exists at low concentrations in extranuclear compartments, and higher concentrations in the ΔNLS Wld^S variant, consistent with a direct axonal role for Wld^S.

Materials and Methods

In vitro/in vivo *expression of Wld^S variants*

To reduce Wld^S nuclear targeting, arginines 213 and 215 were mutated to alanine using the Stratagene QuikChange Site-Directed Mutagenesis Kit and the Wld^S transgene construct (Mack et al., 2001) as template. The two primers used were exactly reverse complementary, the forward primer having the following sequence (R→A encoding mutations underlined): 5′-GCACTGGAAAAGCCTGGGGCGAAGGCGAAGTGGGCTGATCAAAAG-3′.

The sequence contained in pBluescript CK+ (Stratagene) was verified and subcloned into pHβ-Apr1 containing β-actin promoter (Mack et al., 2001) or into pcDNA3 vector (Invitrogen). For *in vitro* expression of variant Wld^S EGFP fusion proteins, the ΔNLS^{R213A,R215A} Wld^S cDNA was amplified by high-fidelity PCR from the above construct using *Bam*HI- and *Hin*dIII-tagged primers and subcloned in-frame to the EGFP sequence into pEGFP-N1 vector (BD Bioscience).

For generation of ΔNLS Wld^S transgenic mice, the ΔNLS^{R213AR215A} Wld^S cDNA including β-actin promoter from above pHβ-Apr1 vector was linearized using *Eco*RI and *Nde*I restriction enzymes and pronuclear injection of the fragment into an F1 C57BL/CBA strain was performed by the in-house Gene Targeting Facility of the Babraham Institute. Eleven founder mice for the ΔNLS Wld^S strain and their transgene-positive offspring were identified by Southern blotting of *Bam*HI plus *Hin*dIII double-digested genomic tail DNA hybridized with a ^{32}P-labeled Wld^S cDNA probe and by PCR using appropriate primers. Founders with medium to high copy number integrations were selected for further study (to generate transgenic lines 1–8) and crossed to homozygous YFP-H mice (The Jackson Laboratory) to breed mice hemizygous for the ΔNLS^{R213AR215A} Wld^S and YFP transgene. Subsequently, these mice were intercrossed to obtain mice homozygous for the ΔNLS^{R213AR215A} Wld^S and positive for the YFP transgene. Mice positive for the YFP transgene were identified by Southern blotting using a ^{32}P-labeled YFP cDNA probe. Furthermore, we used double heterozygous native Wld^S/YFP-H mice, triple heterozygous tg-Wld^S/Wld^S/YFP-H mice, homozygous natural Wld^S mice, and homozygous Wld^S transgenic rats from line 79 (Adalbert et al., 2005) for this study. Triple heterozygous tg-Wld^S/Wld^S/YFP-H mice express levels of Wld^S protein similar to those of homozygous natural mutant Wld^S mice and display a similarly retarded time course of axon degeneration (Beirowski et al., 2005).

Cell culture

Culture and transfection of PC12 and HeLa cells using Lipofectamine 2000 (Invitrogen) was performed as described previously (Wilbrey et al., 2008). Dissociated hippocampal and DRG neuron cultures were prepared from embryonic day 14.5 (E14.5)–E16.5 mouse embryos and transfected using Lipofectamine LTX with PLUS reagent (Invitrogen) as described previously (Conforti et al., 2007; Wilbrey et al., 2008). Cells were plated on 35 mm Petri dishes (μ-Dish, ibidi) for subsequent labeling experiments and high-resolution confocal imaging. For mitochondrial colocalization studies, transfected neurons were treated with 40 nM Mitotracker Red CMXRos (Invitrogen) for 30 min according to the manufacturer's instructions for live cell staining. Additionally, the pDsRed2-Mito vector (Clontech, PT3633-5) was used for mitochondrial labeling.

For SCG explant cultures SCGs were dissected from 1- or 2-d-old mouse pups using sterile technique. Explants were placed into L15 (Leibovitz) medium (Invitrogen) containing 0.01% fetal bovine serum for removal of other tissue, and three explants were then placed in the center of 3.5 cm tissue culture dishes precoated with poly-L-lysine (20 μg/ml for 2 h; Sigma) and laminin (20 μg/ml for 2 h; Sigma). Explants were cultured in DMEM containing 4500 mg/L glucose and 110 mg/L sodium pyruvate (Sigma), 2 mM glutamine, 1% penicillin/streptomycin, and 100 ng/ml 7S NGF (all from Invitrogen), 20 μM uridine and fluorodeoxyuridine (both Sigma) to block proliferation of non-neuronal cells, and 10% fetal bovine serum (Sigma). After 7 d in culture, explants and their radial neurite networks from three dishes were separated by transection and collected separately for lysis directly in Laemmli sample buffer. Explant fractions contain the cell bodies and proximal neurites while the distal neurite fraction is almost exclusively neurites.

For dissociated cultures, explants were treated as described previously (Whitfield et al., 2004). Approximately 10,000 dissociated neurons were plated in a 1 cm^2 area of a laminin-coated 35 mm Petri dish (μ-Dish, ibidi) and maintained under the same conditions as above.

Biochemical assessment of variant Wld^S protein levels

Brains, lumbar spinal cord, and sciatic nerve segments were homogenized in RIPA buffer and prepared for Western blotting as previously described (Mack et al., 2001; Conforti et al., 2007).

Subcellular fractionation was as previously published with modifications (Spencer et al., 2000; Okado-Matsumoto and Fridovich, 2001; Liu et al., 2004; Fang et al., 2005). In initial experiments for generation of crude nuclear, cytoplasmic, and cytosolic fractions (see Fig. 2*A*) mouse brains were snap-frozen by immersion in liquid nitrogen and stored on dry ice. The nuclear transcription factor SP1 and β-actin served as nuclear and cytoplasmic markers respectively and as loading controls for these respective fractions (Sau et al., 2007).

Each brain was homogenized using a Teflon-glass pestle (no. B15541, Thomas; 10 strokes, 700 rpm) at 1:5 (w/v) ratio in ice-cold homogenization buffer containing 10 mM HEPES, 6 mM $MgCl_2$, 1 mM EDTA, 10% sucrose, pH 7.2, and protease inhibitor cocktail (Roche Diagnostics). Unbroken cells and connective tissue were removed by filtration using a cell strainer (40 μm nylon, BD Falcon). Homogenized brain tissue was centrifuged at 2000 × *g* for 5 min. Further centrifugation of the resulting pellet A and supernatant B at different speeds yielded the following fractions.

Nuclear fraction. The pellet A was washed repeatedly and finally resuspended in 0.25 ml of homogenization buffer containing additionally 0.5 M NaCl. The suspension was then incubated for 1 h in an ice bath with frequent vortexing. After incubation the suspension was centrifuged at 8000 × *g* for 10 min, and the final supernatant was regarded as nuclear fraction.

Cytoplasmic fraction. The supernatant B was further centrifuged at 8000 × *g*, and the final supernatant was used as cytoplasmic fraction.

Cytosolic fraction. The supernatant B was centrifuged at 100,000 × *g* for 30 min, and the final supernatant was regarded as cytosolic fraction.

In follow-up subcellular fractionation experiments for generation of enriched mitochondrial and microsomal preparations (see Fig. 9*A*), mouse and rat brains were homogenized as described above in buffer containing 50 mM Tris, 6 mM $MgCl_2$, 1 mM EDTA, 10% sucrose, pH 7.2, and protease inhibitor cocktail (Roche Diagnostics). After 5 min of centrifugation at 2000 × *g*, the resulting pellet C and supernatant D were used for generation of the following fractions.

Nuclear and postnuclear fraction. The pellet C was resuspended in homogenization buffer plus 0.5 M NaCl for 1 h on ice and the suspension centrifuged at 8000 × *g* for 10 min. The resulting pellet was again resuspended in homogenization buffer and used as nuclear fraction. The supernatant D was centrifuged at 8000 × *g* for 10 min to obtain the postnuclear fraction (supernatant).

Cytoplasmic and mitochondria-enriched fraction. The postnuclear fraction was centrifuged at 21,000 × *g* for 20 min to obtain mitochondria-enriched pellet and cytoplasmic fraction (supernatant). The mitochondria-enriched pellet was washed in homogenization buffer and resuspended in buffer containing 150 mM NaCl, 50 mM Tris/HCl, and 10% SDS, pH 8.0. This final suspension was regarded as mitochondria-enriched fraction.

Microsome-enriched and cytosolic fraction. The cytoplasmic fraction was centrifuged at 135,000 × *g* for 1 h to obtain the microsome-enriched fraction (pellet) and cytosolic fraction (supernatant). The microsome-enriched pellet was processed in the same way as the mitochondria-enriched pellet to obtain the final microsome-enriched fraction.

All described centrifugation steps were performed at 4°C using a Sanyo MSE Harrier 18/80 and Beckman MAX Ultracentrifuge. Subcellular fractions were stored at −80°C and subsequently used for Western blot analysis.

For Western blotting SDS-PAGE and standard wet protein transfer (Bio-Rad) to PVDF membranes were performed as previously described with modifications (Mack et al., 2001; Conforti et al., 2007). Variant Wld^S was detected using rabbit polyclonal antiserum Wld18 (1:2000) with mouse monoclonal anti-β-actin (1:3000, Abcam, ab8226) or mouse monoclonal anti-neuronal class βIII-tubulin (1:2000, Covance, MMS-435P) as loading controls. In fractionation experiments the following antibodies were used as loading controls: mouse monoclonal anti-SP1 (1:1000, Santa Cruz Biotechnology, PEP2 sc-59); mouse monoclonal anti-histones H1 (1:500, Chemicon International, MAB052); and mouse monoclonal anti-COXIV (1:5000, Abcam, ab14744).

For quantification, integrated optical density (OD) of bands from three blots per experimental group was determined by NIH ImageJ software, normalized to the loading controls and expressed as a percentage of reference Wld^S expression level.

Nmnat enzyme activities from sagittally divided half mouse brains were determined as described previously (Conforti et al., 2007).

Assessment of axon preservation

All experiments were performed in accordance with the Animals (Scientific Procedures) Act, 1986, under Project License PPL 80/1778. Mice were anesthetized by intraperitoneal injection of Ketanest (5 mg/kg; Parke Davis) and Rompun (100 mg/kg; Bayer). Right sciatic nerves were transected or crushed close to the "foramen intrapiriforme" with contralateral side as control. A 5 mm segment was removed to prevent regeneration from complicating analysis of degeneration at longer lesion durations (14–49 d). The lesion site was also inspected upon nerve removal to be sure the proximal and distal stumps had been fully separated and remained separate. After 6 h (for crush experiments) and 3, 5, 14, 21, 28, 35, and 49 d (for transection experiments), the mice were humanely killed and sciatic/tibial nerve segments were dissected.

We tested the structural preservation of axons in the sciatic and tibial nerve following unilateral sciatic nerve transection by confocal microscopy of a YFP-labeled axonal subset (longitudinal imaging) and by light/electron microscopy using highly established methods for evaluation of axon integrity (Mack et al., 2001; Beirowski et al., 2004, 2005; Adalbert et al., 2005; Conforti et al., 2007).

For analysis of axonal preservation in YFP-labeled nerves, ~1.5-cm-long nerve stumps containing the sciatic and tibial nerve segments were dissected from humanely killed mice following sciatic nerve transection, processed as previously described (Beirowski et al., 2004, 2005), and mounted on conventional glass slides in Vectashield mounting medium for subsequent analysis on a Zeiss LSM 510 Meta Confocal system. Confocal *z*-stack series from both longitudinally embedded sciatic and tibial nerve were taken using a 20× magnification objective, and *z*-projections were electronically generated for final presentation. Criteria for survival were unfragmented YFP-positive fibers in the analyzed segment.

For semithin light microscopy and electron microscopy, sciatic and tibial nerve segments were fixed for at least 3 d in 0.1 M phosphate buffer containing 4% paraformaldehyde and 2.5% glutardialdehyde, embedded in Durcupan resin (Fluka), and processed as described previously (Conforti et al., 2007). Morphological criteria for intact axons were normal myelin sheaths, uniform axoplasm, and intact mitochondria. The percentage of surviving axons in nerve segments was calculated in relation to unlesioned preparations.

Electrophysiology and vital labeling of neuromuscular junctions

Mice were killed by cervical dislocation. Previous section of the sciatic nerve was verified by reexposing the wound in the thigh. Tibial nerve–flexor digitorum brevis (FDB) preparations were dissected and pinned to a Sylgard-lined dish and bathed in oxygenated mammalian physiological saline (137 mM Na^+, 4 mM K^+, 2 mM Ca^{2+}, 1 mM Mg^{2+}, 147 mM Cl^-, 5 mM glucose, and 5 mM HEPES, pH 7.2–7.4, equilibrated with 100% oxygen). The nerve was stimulated using a suction electrode connected to a Powerlab 4/20T and stimulated using 50–200 μs pulses, 0.1–1 mA intensity at 1–20 Hz. Muscle contractions were recorded as short (10–35 s) movies through a Wild M5A dissecting microscope using a Nikon Coolpix 4500 digital cameral fitted with an ocular adapter. The three distal tendons of FDB were then tied together using Ethicon 7/0 suture and connected to a Grass force transducer and the Powerlab bridge amplifier. Twitch contractions to single stimuli delivered at 1–5 Hz and fused contractions evoked by 20 Hz stimulation were recorded using Chart v4.1.1 and Scope v3.6.8 software on an Apple Macintosh Powerbook computer. The preparation was then dismounted from the force transducer and a pair of fine electromyographic recording needles, insulated to within 0.2 mm of their tips with a coating of nail varnish, was inserted into the belly of the FDB muscle. The bathing solution was earthed (grounded) using an Ag/AgCl wire and all three electrodes were connected to the Bioamp input of the Powerlab unit. Stimuli to the tibial nerve were delivered either from the Powerlab using parameters indicated above, or using a A-M Systems 210 isolated pulse stimulator with variable 1–10 V pulses, 200 μs in duration and at frequencies of 1–40 Hz. EMG signals were low-pass (2 kHz), high-pass (10 Hz), 50 Hz notch, and mains filtered and averaged using Scope software. In some cases, a simpler preparation was used for EMG recording. Isolated hindlimbs were stripped of their skin and pinned to a Sylgard-lined dish in oxygenated mammalian saline as above. The tibial nerve was dissected free to the ankle, the foot was amputated at the tibia, and EMG needles were inserted immediately into the FDB/interosseous muscles. The tibial nerve was stimulated with a suction electrode and the EMG response recorded and averaged using the Powerlab Scope software. Sample records were extracted from the Chart and Scope raw data files and pasted into Powerpoint.

For morphological quantification of functionally preserved neuromuscular junctions (NMJs) in tibial nerve–FDB preparations recycled synaptic vesicles of motor nerve terminals were stained using AM1-43 (Nerve Terminal Staining Kit II, Biotium) with 20 Hz nerve stimulation. AM1-43 is a fixable form of styryl dye FM1-43, widely used for vital labeling of NMJs, where it indicates functional synaptic transmission (Betz et al., 1992; Barry and Ribchester, 1995; Mack et al., 2001). Unspecific background fluorescence of AM1-43 was quenched with ADVASEP-7 (Kay et al., 1999). Acetylcholine receptors were subsequently stained with tetramethylrhodamine isothiocyanate conjugates of α-bungarotoxin (TRITC-α-BTX) (Biotium). FDB muscles were fixed in 0.1 M PBS containing 4% paraformaldehyde for 30 min, cleaned of connective tissue and mounted on conventional glass slides in Vectashield mounting medium for analysis. For quantification of endplate occupancy following sciatic nerve lesion occupied and vacant bungarotoxin-labeled NMJs in the three subcompartments of the FDB muscle (see supplemental movies, available at www.jneurosci.org as supplemental material) were counted using an IX81 Olympus fluorescence microscope. Fifty to one hundred endplates were assessed per FDB preparation and compared with the contralateral unlesioned preparation from each mouse.

Immunocytochemistry and immunohistochemistry

For conventional indirect immunofluorescence detection of Wld^S variant expression in primary and secondary cell culture, cells were fixed in 4% paraformaldehyde (PFA) 48 h after transfection, permeabilized with 1% Triton X-100 for 10 min, blocked [5% NGS (Sigma) in PBS, 1 h], and immunostained using rabbit polyclonal Wld18 antibody (1:500) and secondary Alexa568-goat anti-rabbit antibody (1:200) diluted in 5% NGS/PBS. Nuclear counterstaining was performed with DAPI and cells were mounted in Vectashield (Vector Laboratories).

For immunofluorescence detection of variant Wld^S protein on brain, lumbar spinal cord, DRG, and sciatic nerve obtained from perfusion fixed mice, 20 μm cryostat sections on poly-L-lysine-coated glass slides (VWR SuperFrost Plus) were incubated overnight in citrate buffer, pH 6.0, at 50°C or for 45 min in 0.05% citraconic anhydride solution, pH 7.4, at 98°C (Namimatsu et al., 2005) and subsequently permeabilized with 0.1% Triton X-100 plus 0.05 M NH_4Cl in 0.05 M TBS for 10 min. The sections were then rinsed in fresh TBS, immunoblocked with 5% bovine serum albumin (Sigma) in TBS for 1 h, and incubated overnight at 4°C in primary antibody solution (Wld18 antibody, 1:500 in 0.8% bovine serum

albumin in TBS). After extensive washes, the secondary antibody solution (Alexa568-goat anti-rabbit, 1:200 in TBS) was applied for 1 h at room temperature and slices were rinsed in TBS and dH_2O. The samples were counterstained with primary mouse monoclonal anti-neuronal class βIII-tubulin (1:500, Covance, MMS-435P), mouse monoclonal anti-neurofilament 200 (1:500, Sigma, clone 52, N0142), or mouse monoclonal anti-APP (1:200, Chemicon, MAB348) and secondary Alexa488-goat anti-mouse (1:200) antibodies as above. Nuclear staining was performed with DAPI or Hoechst 33258. Samples were mounted in Vectashield mounting medium (Vector Laboratories).

For high-sensitivity detection of low-abundance Wld^S protein variants on dissociated SCG and DRG neuronal cultures exploiting catalyzed reported deposition of tyramide-Alexa 488 or tyramide-Alexa 568 conjugate (Molecular Probes TSA detection kit, Invitrogen), cells were fixed for 15 min with 4% PFA in 0.1 M PBS, rinsed, and permeabilized with 1% Triton X-100 for 10 min. After quenching endogenous peroxidase activity with 3% hydrogen peroxide in PBS for 1 h, cells were treated with 1% TSA blocking buffer (Molecular Probes, Invitrogen) for 1 h, and primary antibody Wld18 (1:500 in 1% TSA blocking buffer) was applied overnight at 4°C. Cells were extensively washed in PBS and incubated with HRP-coupled goat anti-rabbit secondary antibody (1:100 in 1% TSA blocking buffer) for 1 h. The tyramide-fluorophore conjugate solution was applied for 10 min according to the manufacturers instructions. Cells were extensively washed and conventionally counterstained with the following primary antibodies: mouse monoclonal anti-neurofilament 200 (1:500, Sigma, clone 52, N0142); mouse monoclonal anti-COXIV (1:100, Abcam, ab14744); mouse monoclonal anti-KDEL (1:100, MAC 256, gift from Geoff Butcher, Babraham Institute, Cambridge, UK); mouse monoclonal anti-LAMP-2 (1:10, ABL-93, gift from Aviva Tolkovsky, University of Cambridge, Cambridge, UK). Secondary Alexa488-goat anti-mouse (1:200) antibodies were applied, and cells were washed in PBS and dH_2O and mounted in Vectashield mounting medium.

For high-sensitivity detection of variant Wld^S on cryostat sections of peripheral and central nerves, ~5 mm sciatic and optic nerve segments were dissected and postfixed for 2 h in 4% PFA in 0.1 M PBS. After extensive PBS washes, the nerves were incubated overnight in 20% sucrose, embedded in OCT embedding medium (Shandon), and frozen in a −80°C freezer. Serial 20 μm cryostat sections were cut and mounted onto poly-L-lysine-coated slides. Sections were incubated at 98°C with 0.05% citraconic anhydride solution, pH 7.4, for 45 min and permeabilized with 0.5 M NH_4Cl + 0.25% Triton in 0.1 M PBS, and low-abundance Wld^S protein was detected using HRP-catalyzed tyramide-fluorophore conjugate deposition as described above. In some experiments, the sections were counterstained with Hoechst 33258 and finally mounted in Vectashield mounting medium.

For nonfluorescence immunohistochemical detection of Wld^S variants, frozen sections were pretreated by incubating overnight at 50°C in citrate buffer, pH 6.0, for antigen retrieval. The Vectastain Elite ABC Kit (PK-6100, Vector Laboratories) was applied according to the manufacturer's instructions, and the peroxidase reaction was visualized with 3,3′-diaminobenzidine (DAB) plus nickel enhancement (ABC method). The WldS18 primary antibody was used at a dilution of 1:500. DAB-labeled sections were counterstained with nuclear fast red (Vector Laboratories).

Nonfluorescent immunohistochemically stained tissue sections were imaged with a Leitz DM RB microscope coupled to a Leica DC camera system and Leica DC Twain Software.

Confocal imaging and fluorescence intensity quantification

Immunostained tissue sections and vital dye-labeled muscle preparations were imaged on a Zeiss LSM 510 Meta Confocal system, and *z*-series were merged using algorithms from Zeiss LSM Software Release 3.2. Colocalization analysis used Multi-track configuration mode to avoid cross talk between individual fluorophores and bleed-through. Object based colocalization analysis was performed by assessment of overlap between linear fluorescence intensity profiles in individual focal planes. Nuclear variant Wld^S expression in lumbar spinal cord motoneurons was measured in the ventral horn (10 motoneurons per mouse). Confocal *z*-series stacks of Hoechst 33258-labeled entire nuclear profiles were recorded and mean variant Wld^S fluorescence intensities were measured on each single optical section using algorithms from Zeiss LSM Software Release 3.2. The measured mean intensities were normalized to reference signal derived from endothelial nuclear profiles without variant Wld^S expression from the same section (nuclei of endothelial cells).

Statistical analysis

Data are presented as mean ± SD. One-way ANOVA was used for group comparisons and statistical significance or high significance was considered if $p < 0.05$ or $p < 0.005$, respectively.

Results

Two point mutations redistribute Wld^S from nucleus to cytoplasm *in vitro*

To reduce targeting of full-length Wld^S protein from nuclei we introduced two point mutations (R213A, R215A) within the NLS of the Nmnat1 domain. We confirmed nuclear Wld^S reduction by transiently transfecting primary hippocampal and dorsal root ganglion (DRG) cultures and HeLa and PC12 cells. Immunofluorescence with Wld18 antibody, directed against the unique linker region in Wld^S (Samsam et al., 2003), showed almost complete exclusion from nuclei in HeLa and PC12 cells and substantially reduced nuclear targeting in primary culture (Fig. 1*A* and data not shown). Thus, the previously identified Nmnat1 NLS (Sasaki et al., 2006) is also the main determinant of nuclear localization of full-length Wld^S protein. We additionally identified a weak predicted NLS (PSORTII and NucPred predictions) within the N-terminal 16 aa of Wld^S but chose not to mutate this region because its influence on Wld^S biochemistry (Laser et al., 2006) could affect phenotype in other ways.

Interestingly, in neurons we detected a strong signal in neuritic trees, especially prominent in neurites >500 μm (Fig. 1*A* and data not shown). This suggests that the ΔNLS Wld^S molecule either diffuses or is transported into neurites *in vitro*. Neuritic immunosignal was not observed in cells expressing native Wld^S using this method.

Generation of transgenic mice overexpressing ΔNLS Wld^S

After testing *in vitro* we coupled the $\Delta NLS^{R213A,R215A}$ Wld^S cDNA to a β-actin promoter, a system that consistently confers a Wld^S phenotype in mice and rats using native Wld^S (Mack et al., 2001; Adalbert et al., 2005). Lines were established from seven of the eight founders (lines 1–6, 8) by breeding to YFP-H mice (Feng et al., 2000) for convenient assay of axon degeneration (Beirowski et al., 2004). Line 3, 6, and 8 hemizygotes showed very similar total brain expression levels to that of Wld^S in heterozygous Wld^S mice, whereas variant Wld^S levels were higher in lines 2 and 5 (Fig. 1*B*). Lumbar spinal cord levels were lower relative to Wld^S heterozygotes in lines 3, 6, and 8. This difference between brain and spinal cord may reflect the increased presence of variant Wld^S in the axon (see below), most of which lies outside the spinal cord. As expected, breeding to homozygosity elevated ΔNLS Wld^S protein expression in brain approximately twofold (data not shown). Variant Wld^S was not detectable in Western blots from lines 1 and 4, even in homozygous mice, probably reflecting insertional silencing. Enzyme assays showed increased Nmnat activity in brains of highly expressing lines broadly in line with these protein concentrations (Fig. 1*C*), also confirming that mutation of the NLS did not impair NAD^+ synthesis efficacy, which is critical for the neuroprotective phenotype (Araki et al., 2004) (L. Conforti, A. Wilbrey, G. Morreale, L. Janeckova, B. Beirowski, R. Adalbert, F. Mazzola, M. Di Stefano, R. Hartley, E. Babetto, T. Smith, J. Gilley, R. Billington, A. Genazzani, R. Ribchester, G. Magni, and M. Coleman, unpublished work).

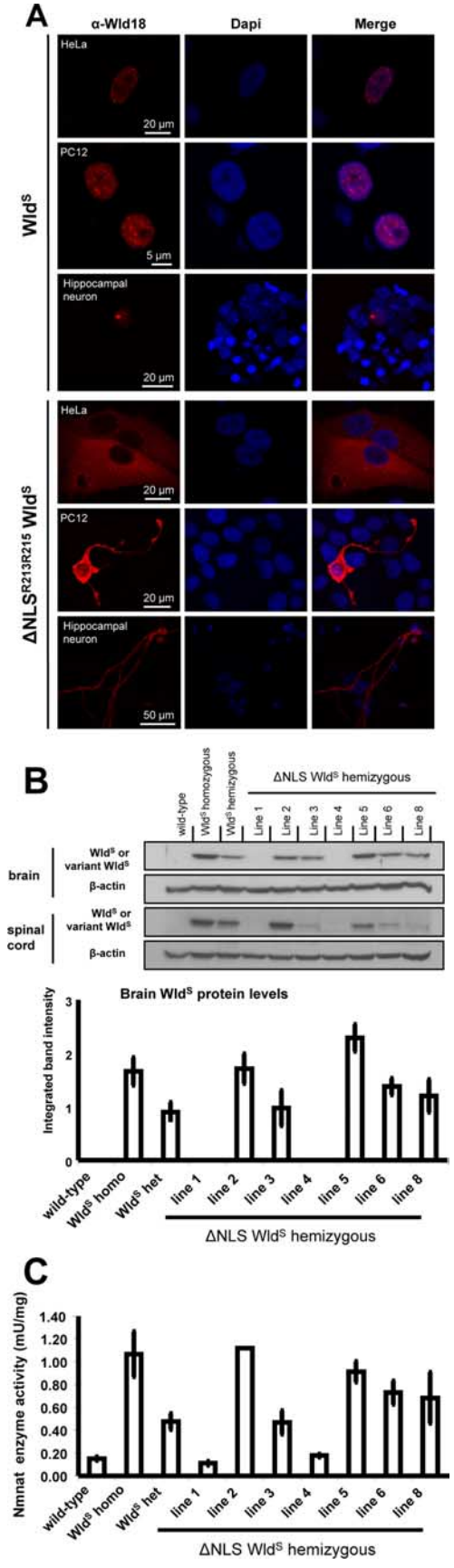

Figure 1. Subcellular localization of ΔNLS Wld^S in different cell types *in vitro* and initial characterization of ΔNLS Wld^S transgenic mice. ***A***, Immunofluorescence using Wld18 primary and Alexa dye-coupled secondary antibodies showing ΔNLS Wld^S cytoplasmic translocation in transfected HeLa and PC12 cells and hippocampal neurons. ***B***, Top, Representative Westerns blots from brain and lumbar spinal cord crude extracts probed with Wld18 antibody and β-actin loading control. Bottom, Intensities of individual variant Wld^S protein Western blot bands from brain were densitometrically quantified and normalized to β-actin loading control ($N = 3$ mice for each group tested). ***C***, Normalized brain Nmnat enzyme activities in individual ΔNLS Wld^S transgenic lines, wild-type controls, and Wld^S ($N = 2–8$ mice for each group tested).

NLS mutation reduces nuclear targeting of Wld^S *in vivo*

To assess subcellular redistribution of the ΔNLS Wld^S protein *in vivo*, we performed Western blots of nuclear, cytoplasmic, and cytosolic fractions (Fig. 2*A*). Nuclear targeting was reduced by >90% in brain tissue in all expressing lines relative to native Wld^S (Fig. 2*A*), although curiously cytoplasmic levels were consistently increased only in transgenic line 5. This could reflect the enormous dilution upon redistribution from nucleus to the much larger cytoplasmic compartment, especially in projection neurons. We were surprised to find significant quantities of native Wld^S in cytoplasm, but this may have been missed previously due to the use of paraffin-embedded sections, sometimes a less specific antibody (Mack et al., 2001), and Western blotting of just one brain region (cortex) (Fang et al., 2005). In accordance with earlier results (Fang et al., 2005), however, we did not detect Wld^S in cytosol.

Immunofluorescence of brain and lumbar spinal cord frozen sections also showed strongly reduced nuclear targeting (Fig. 2*B*). In some cortical and cerebellar neurons, confocal imaging showed only very faint nuclear Wld^S staining (Fig. 2*B*, rows 1–4). Faint signals in motor neuron nuclei (Fig. 2*B*, rows 5–7) were highly significantly reduced in multiple lines relative to spontaneous Wld^S mice (Fig. 2*C*). Reflecting variant Wld^S redistribution, a faint outline of individual cell bodies was readily visible in homozygotes of lines 2 and 3 (Fig. 2*B*, row 6, arrows). Similar redistribution with reductions in nuclear targeting was seen in DRG neurons (supplemental Fig. 1, available at www.jneurosci.org as supplemental material).

Using 3,3′-diaminobenzidine immunostaining on frozen sections, we found clear Wld^S cytoplasmic signals in ΔNLS Wld^S spinal cord motorneurons with distinct labeling of proximal neuronal processes (Fig. 2*B*, row 7, asterisks). Interestingly, we also could detect weak cytoplasmic variant Wld^S signals in some motorneurons from ΔNLS line 1 this way, suggesting the transgene is expressed in this line but at a very low level.

Thus, ΔNLS Wld^S transgenic lines express the variant Wld^S protein with full Nmnat enzyme activity and considerably reduced nuclear targeting and relative cytoplasmic redistribution in various neuronal subtypes.

ΔNLS Wld^S delays Wallerian degeneration more robustly than native Wld^S

We and others have previously shown that delay of Wallerian degeneration and related axon pathologies by Wld^S is strongly dose dependent (Perry et al., 1990; Mack et al., 2001; Samsam et al., 2003; Adalbert et al., 2005). In particular, the strength of axon protection in transgenic mice correlates closely with Wld^S protein level (Mack et al., 2001) (and unpublished observations) (note: the lower expressing lines are no longer available for comparison). Thus, if Wld^S works through an intranuclear mechanism, reducing nuclear targeting should weaken the protective phenotype.

Surprisingly, however, axonal continuity was substantially better preserved 3, 5, and 14 d after nerve lesion in ΔNLS Wld^S transgenic lines 2, 3, 5, 6, and 8 than in native Wld^S mice (Fig. 3*A* and data not shown). Fragmentation in wild type and partial fragmentation in Wld^S heterozygotes (Fig. 3*A*, asterisks) was not

←

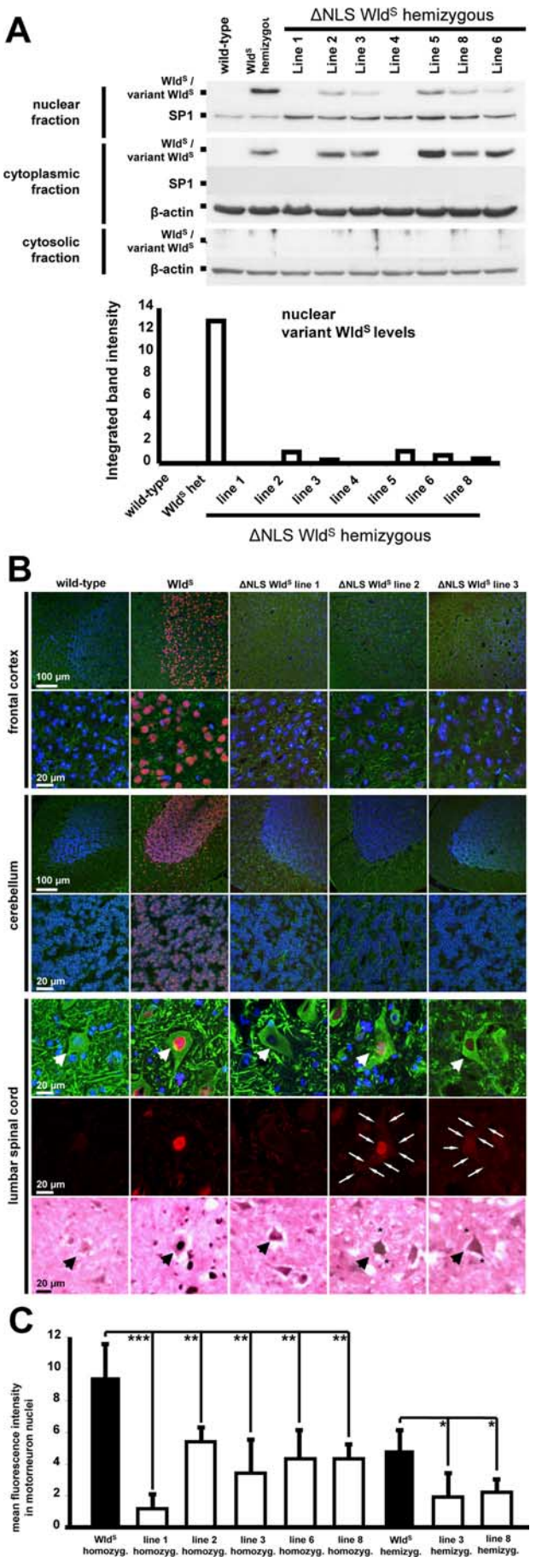

seen in hemizygous ΔNLS Wld^S transgenics. Similar results were obtained in transverse semithin sections 3–14 d after nerve lesion (Fig. 3*B*; supplemental Fig. 2, available at www.jneurosci.org as supplemental material). Quantification showed significantly to highly significantly more intact axons in line 2, 3, 5, 6, and 8 hemizygotes than in Wld^S heterozygotes ($p < 0.05$ and $p < 0.005$, one-way ANOVA). For example, after 14 d, 24.2 ± 2.2% intact axons were intact in Wld^S ($N = 3$) compared with 67.4 ± 2.8% in line 3 ($N = 3$).

Intriguingly, lines 1 and 4 showed axon preservation up to 14 d (supplemental Fig. 3, available at www.jneurosci.org as supplemental material, and data not shown) despite the lack of detectable variant Wld^S on Western blots (Fig. 1*B*). In contrast, we previously reported that a low but detectable level of native Wld^S was insufficient to confer any detectable axon protection (Wld^S transgenic line 4839 hemizygotes) (Mack et al., 2001). Thus, the amount of protein expressed in transgenic Wld^S line 4839 should be at least as great, while axon protection is far weaker than in ΔNLS Wld^S lines 1 and 4. Unfortunately the previously generated Wld^S line 4839 is no longer available for direct comparison, but this result also suggests Wld^S has greater efficacy after a reduction in nuclear targeting.

Reduction of Wld^S nuclear targeting extends the maximum preservation of axon continuity and ultrastructure

We then asked whether the maximum time for which axon continuity and ultrastructure can be preserved increases when Wld^S nuclear targeting is reduced. For this we used lines 3 and 8 with expression levels similar to native Wld^S mice. In Wld^S heterozygotes all axons degenerated by 21 d, whereas in line 3 ΔNLS Wld^S transgenics some axons remained continuous for at least 35 d (Fig. 4*A*). In homozygotes the maximum preservation of continuous axons was extended from <35 to >49 d (Fig. 4*B* and data not shown). It is also interesting to note that YFP has a sufficiently long half-life in these axons to give a strong signal for 7 weeks after being isolated from any further synthesis in the cell body. To confirm that the loss of signal in Wld^S is not simply due to degradation of YFP, and to study the underlying axon ultrastructure, we then performed electron microscopy at these time points (Fig. 4*C*). Many ultrastructurally normal axons were preserved up to 49 d in ΔNLS Wld^S lines 3 and 8, with uniformly distributed axoplasm and unswollen mitochondria, whereas all axonal profiles were completely degraded in spontaneous Wld^S mice (Fig. 4*C*).

Denervated ΔNLS Wld^S axons and neuromuscular junctions remain functional in young and aged transgenics

To test whether NMJs were also preserved after axotomy, we recorded muscle contractions, electromyography, and vital label-

←

Figure 2. Reduced nuclear targeting of ΔNLS Wld^S in various neuronal subtypes *in vivo*. ***A***, Western blots of nuclear, cytoplasmic, and cytosolic brain fractions demonstrating dramatically reduced nuclear targeting in individual mice from different ΔNLS Wld^S lines compared with spontaneous Wld^S mutant. The bottom graph demonstrates corresponding relative optic densities of nuclear Wld^S bands normalized to SP1 for individual mice. These Western blots are representative of three individual experiments. ***B***, Rows 1–6, Confocal images showing (variant) Wld^S protein immunolabeling (red) with β-III tubulin (green) and Hoechst 33258 (blue) counterstaining on frozen sections from homozygous mice. Transgenics shown represent lines without detectable variant Wld^S protein expression in Western blotting (line 1) and with strong (line 2) and medium (line 3) variant Wld^S protein expression levels. Row 7, Light microscopic pictures from lumbar motorneurons (arrows) showing Wld^S immunolabeling using 3,3′-diaminobenzidine. ***C***, Graph showing normalized fluorescence intensities for nuclear variant Wld^S protein signals in lumbar motoneurons. For each genotype group, three mice were assessed (10 motorneurons each). *$p < 0.05$; **$p < 0.005$; ***$p < 0.001$; one-way ANOVA.

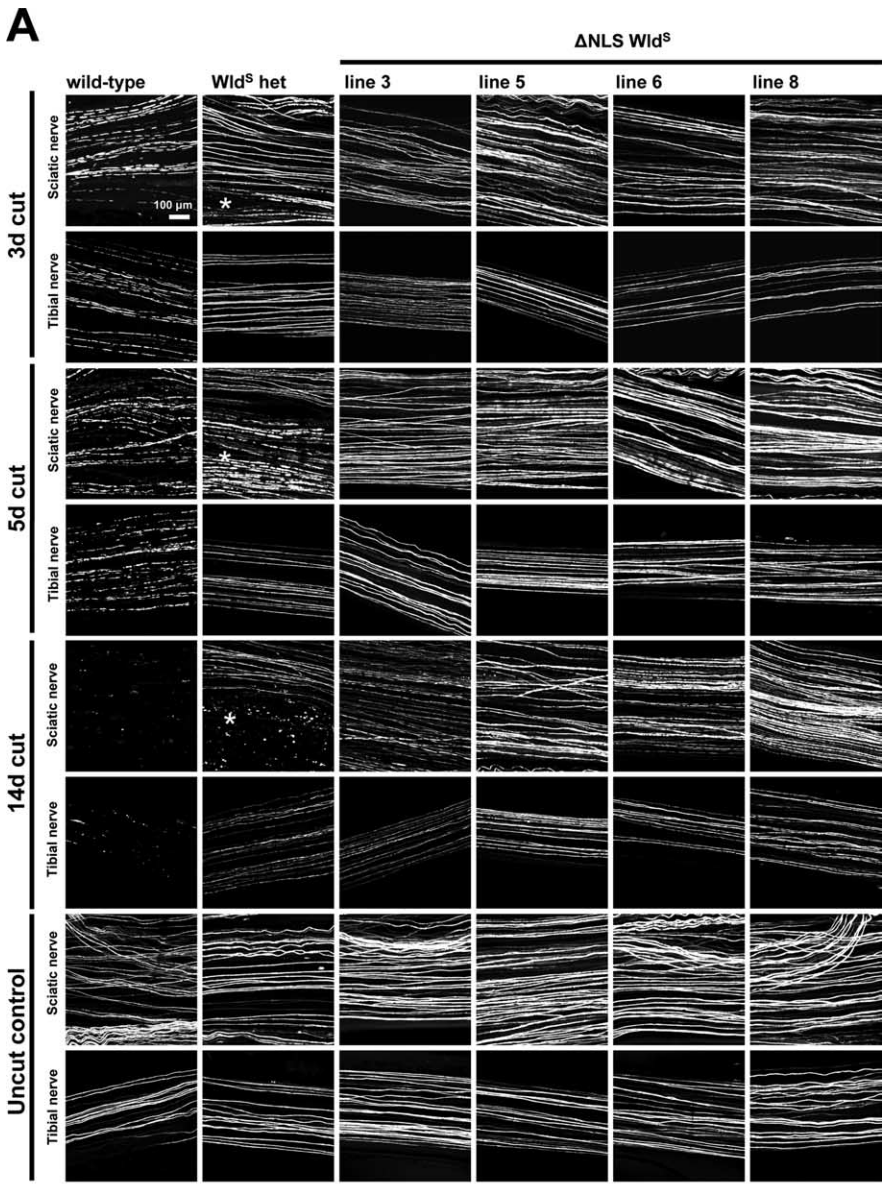

B

Percentage of intact myelinated sciatic nerve axons (% of intact control nerve)

	3 days	5 days	14 days
wild-type	2.4 ± 0.9% (N=3)	0.5 ± 0.4% (N=3)	0.0 ± 0.0%(N=3)
Wld^S het	78.8 ± 3.4% (N=3)	59.2 ± 3.5% (N=3)	24.2 ± 2.2% (N=3)
ΔNLS Wld^S hemi: Line 2 het	95.9 ± 5.0% (N=3)	83.0 ± 10.4% (N=3)	70.2% (N=1)
ΔNLS Wld^S hemi: Line 3 het	99.7 ± 1.1% (N=3)	93.0 ± 2.3% (N=3)	67.4 ± 2.8% (N=3)
ΔNLS Wld^S hemi: Line 5 het	102.4 ± 2.8% (N=3)	91.0 ± 1.3% (N=3)	69.7 ± 2.2% (N=3)
ΔNLS Wld^S hemi: Line 6 het	97.6 ± 16.6% (N=3)	88.6 ± 6.0% (N=3)	68.0 ± 11.3% (N=3)
ΔNLS Wld^S hemi: Line 8 het	103.1 ± 5.1% (N=3)	95.3 ± 2.8% (N=3)	58.4 ± 6.6% (N=3)

Figure 3. Time course of Wallerian degeneration in ΔNLS Wld^S/YFP-H transgenics at 3, 5, and 14 d following sciatic nerve transection. ***A***, Representative confocal *z*-series stacks of sciatic and tibial nerves from wild type, heterozygous Wld^S ("Wld^S het"), and ΔNLS Wld^S transgenics ("ΔNLS Wld^S het") additionally expressing YFP in a representative axonal subset (YFP-H transgene) to facilitate longitudinal imaging of axons 3, 5, and 14 d after transection. No interruptions are detectable in hemizygous ΔNLS Wld^S nerves, whereas axons in nerves from Wld^S heterozygotes increasingly fragment at the indicated time points (asterisks). Note that we observed proximo-distal gradients of axonal fragmentation along the sciatic/tibial nerve consistent with earlier data (Beirowski et al., 2005). ***B***, Quantification of axonal preservation following nerve lesion in semithin sections showing percentage of intact myelinated sciatic nerve axons (percentage of contralateral unlesioned nerve) at 3, 5, and 14 d following axotomy (see supplemental Fig. 2, available at www.jneurosci.org as supplemental material).

ing of synaptic terminals in FDB preparations. Functional protection of axotomized motor nerve terminals and NMJs in spontaneous and transgenic Wld^S mice is highly age dependent, with innervation 3 d after a nerve lesion falling from >80% at 1–2 months to <20% at 12 month (Gillingwater et al., 2002). As expected, young *Wld^S* homozygotes (~2 months) showed robust conduction of action potentials and synaptic transmission 3 and 6 d after axotomy, but this protective phenotype was almost completely lost in older mice (aged >7 months).

Three days after sciatic nerve transection, 2-month-old wild-type FDB muscles showed no activity, while age-matched FDB from ΔNLS Wld^S line 3 or spontaneous Wld^S mutants showed robust contractile and electromyographic responses to nerve stimulation indicating functional preservation of both motor axons and NMJs (supplemental Fig. 4*A–F*, Movies 1, 2, available at www.jneurosci.org as supplemental material). Quantitative, functional labeling using the activity-dependent nerve terminal dye AM1-43 showed almost 100% innervated NMJs in FDB preparations from both ΔNLS Wld^S and spontaneous Wld^S mutants (supplemental Fig. 4*G*, available at www.jneurosci.org as supplemental material). Six days after sciatic nerve transection the proportion of occupied NMJs decreased to ~50% in young Wld^S mutants, whereas young ΔNLS Wld^S transgenics still showed almost 100% intact NMJs, indicating stronger protection of synaptic terminals (Fig. 5*E*; supplemental Fig. 4*G*, available at www.jneurosci.org as supplemental material). After 10 d, <10% of intact NMJs remained in ΔNLS Wld^S FDB (supplemental Fig. 4*G*, available at www.jneurosci.org as supplemental material).

We then studied mice aged 6–12 months old (Fig. 5), when native Wld^S mice almost completely lose neuromuscular synaptic protection. As expected, 7.5-month-old Wld^S muscles showed only weak or no contraction upon stimulation of the axotomized distal nerve stump (supplemental Movie 4, available at www.jneurosci.org as supplemental material; Fig. 5*B*). Electromyographic responses were also very weak (Fig. 5*D*). AM1-43 functional labeling in a 6-month-old Wld^S mutant confirmed almost complete absence of occupied NMJs (Fig. 5*E*). In marked contrast, axotomized FDB from 7.5-month-old ΔNLS Wld^S mice showed robust contractions after nerve stimulation, with contractile forces and electromyographic responses indistinguishable

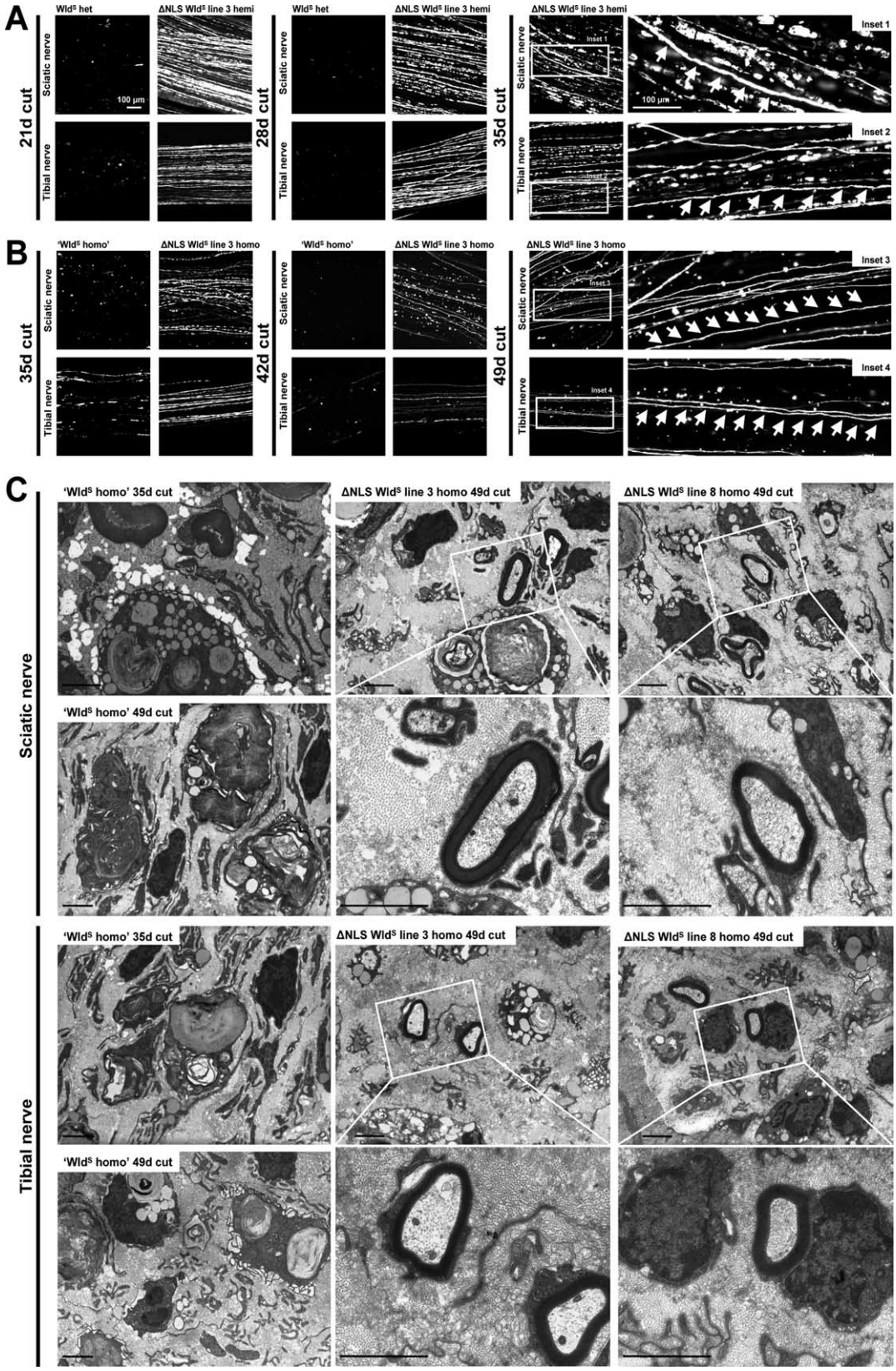

Figure 4. Long-term axon survival after sciatic nerve lesion in ΔNLS Wld^S transgenics. ***A***, Representative confocal images of lesioned sciatic/tibial nerves from heterozygous Wld^S ("Wld^S het") and hemizygous ΔNLS Wld^S transgenics from line 3 crossed to YFP-H. While sciatic and tibial nerves from Wld^S heterozygotes show pronounced degradation of YFP-positive axon fragments from 21 d, ΔNLS Wld^S line 3 hemizygotes have uninterrupted axons up to 35 d (arrows in inset 1 and 2). ***B***, Representative confocal images of lesioned sciatic/tibial nerves from Wld^S ("Wld^S homo") and ΔNLS Wld^S line 3 homozygotes. While Wld^S homozygotes show pronounced degradation of YFP-positive axon fragments from 35 d, ΔNLS Wld^S line 3 mice display uninterrupted axons up to 49 d (arrows in inset 3 and 4). ***C***, Transmission electron microscopy of distal sciatic and tibial nerve from Wld^S homozygotes (left) and line 3 (middle) and line 8 (right) ΔNLS Wld^S transgenics 35 and 49 d following nerve section. In contrast to Wld^S, some ΔNLS Wld^S axons 49 d after axotomy are ultrastructurally preserved, showing intact myelin sheaths, uniform, regularly spaced cytoskeleton, and normal-appearing mitochondria. Scale bars, 2 μm.

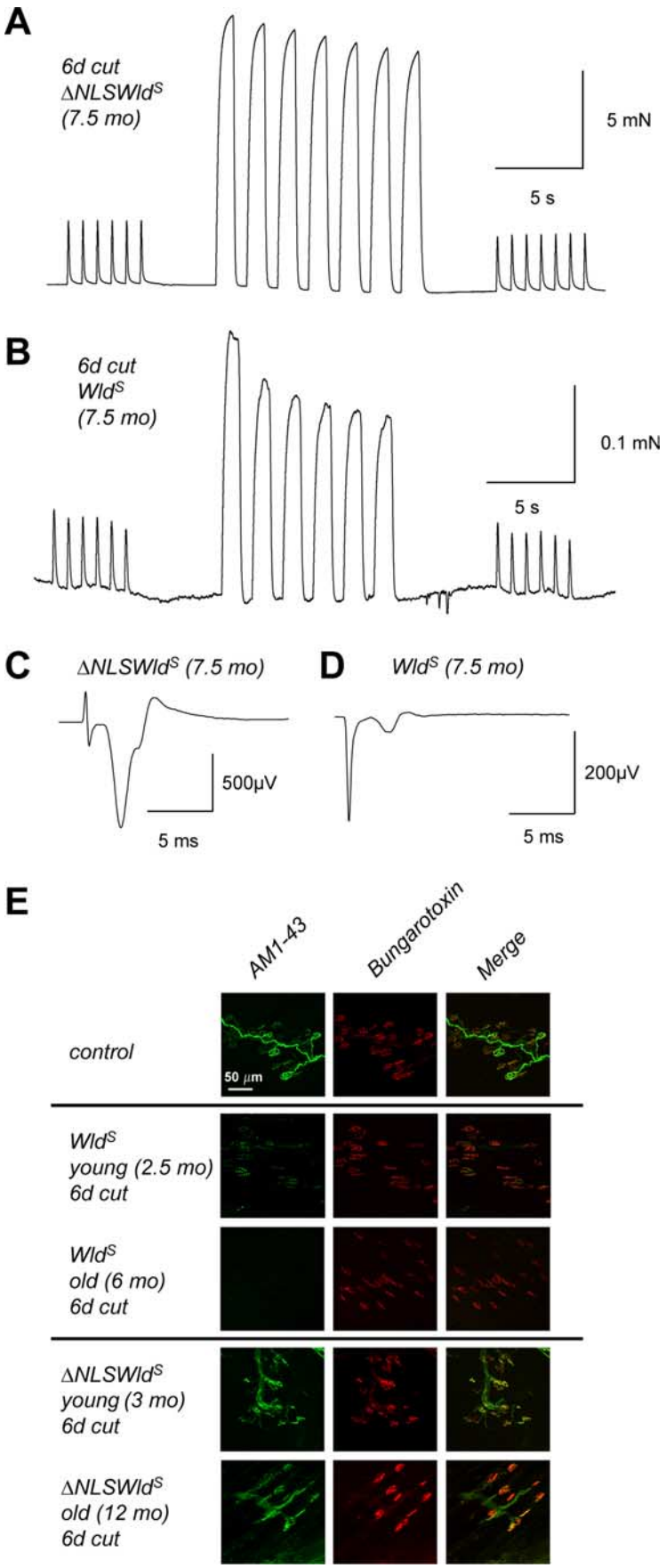

Figure 5. Maintained preservation of neuromuscular function in aged ΔNLS Wld^S transgenic mice. ***A***, ***B***, Recordings of FDB repetitive 1 Hz muscle twitch contractions and 20 Hz fused contractile responses, 6 d after sciatic nerve lesion from 7.5-month-old ΔNLS Wld^S transgenic (***A***) and age-matched native Wld^S mutant (***B***). Note the amplitude of isometric force generated by nerve stimulation in ΔNLS Wld^S is ~50 times that of the native Wld^S. The fluctuating baseline discernible in ***B*** is due partly to the increased amplifier gain required to register the muscle response and partly to distributed asynchronous spontaneous contractions typically observed in axotomized Wld^S muscle. ***C***, ***D***, Averaged extracellular EMG recordings using nerve/muscle preparations from ***A*** and ***B***. The initial spike is the stimulus artifact and the slower waves are produced by muscle fiber action potentials. Note the ~10-fold greater amplitude of the evoked EMG response in ΔNLS Wld^S (***C***) compared with Wld^S (***D***). ***E***, Representative confocal *z*-series projections of paraformaldehyde-fixed FDB nerve muscle preparations double labeled presynaptically with the activity-dependent nerve terminal dye AM1-43 and postsynaptically by the acetylcholine receptor marker TRITC-α-bungarotoxin. Colocalization of the green and red signals thus indicates functionally preserved NMJs.

from nonaxotomized muscles ($N = 2$) (supplemental Movie 3, available at www.jneurosci.org as supplemental material; Fig. 5*A*,*C*). In accord with these results, quantitative AM1-43 functional labeling in a 12-month-old ΔNLS Wld^S mouse 6 d after lesion revealed 95% endplate occupancy (Fig. 5*E*). Together, these results suggest that the decline of synaptic protection with age in native Wld^S mice is significantly reduced by extranuclear targeting of variant Wld^S. Thus, functional survival of motor axons and their nerve terminals increases and becomes independent of age if Wld^S is partially translocated from the nucleus to the cytoplasm *in vivo*.

Detection of Wld^S protein variants in axons

These findings raise the possibility that even native Wld^S protein may function within axons. Western blotting with Wld18 at a dilution at which it is completely specific for Wld^S revealed a faint 43 kDa band in Wld^S mouse and transgenic Wld^S rat sciatic nerves that was absent in wild type (Fig. 6*A*,*B*). Consistent with a local protective action in axons, ΔNLS Wld^S transgenic mice showed substantially higher amounts in nerve extracts from lines 3 and 8 (Fig. 6*A*). Nevertheless, we could see no Wld^S-specific conventional immunofluorescence staining on sections or whole-mount preparations from paraformaldehyde fixed PNS and CNS tissue (data not shown). Interestingly, antigen retrieval using citraconic anhydride (Namimatsu et al., 2005) revealed a marked glial signal in sciatic and optic nerve sections from native Wld^S mice and rats and ΔNLS Wld^S transgenics (Fig. 6*C* and data not shown). This signal increased near the lesion site in injured nerves (Fig. 6*D*), but its significance for axon protection is unknown since neuronal expres-

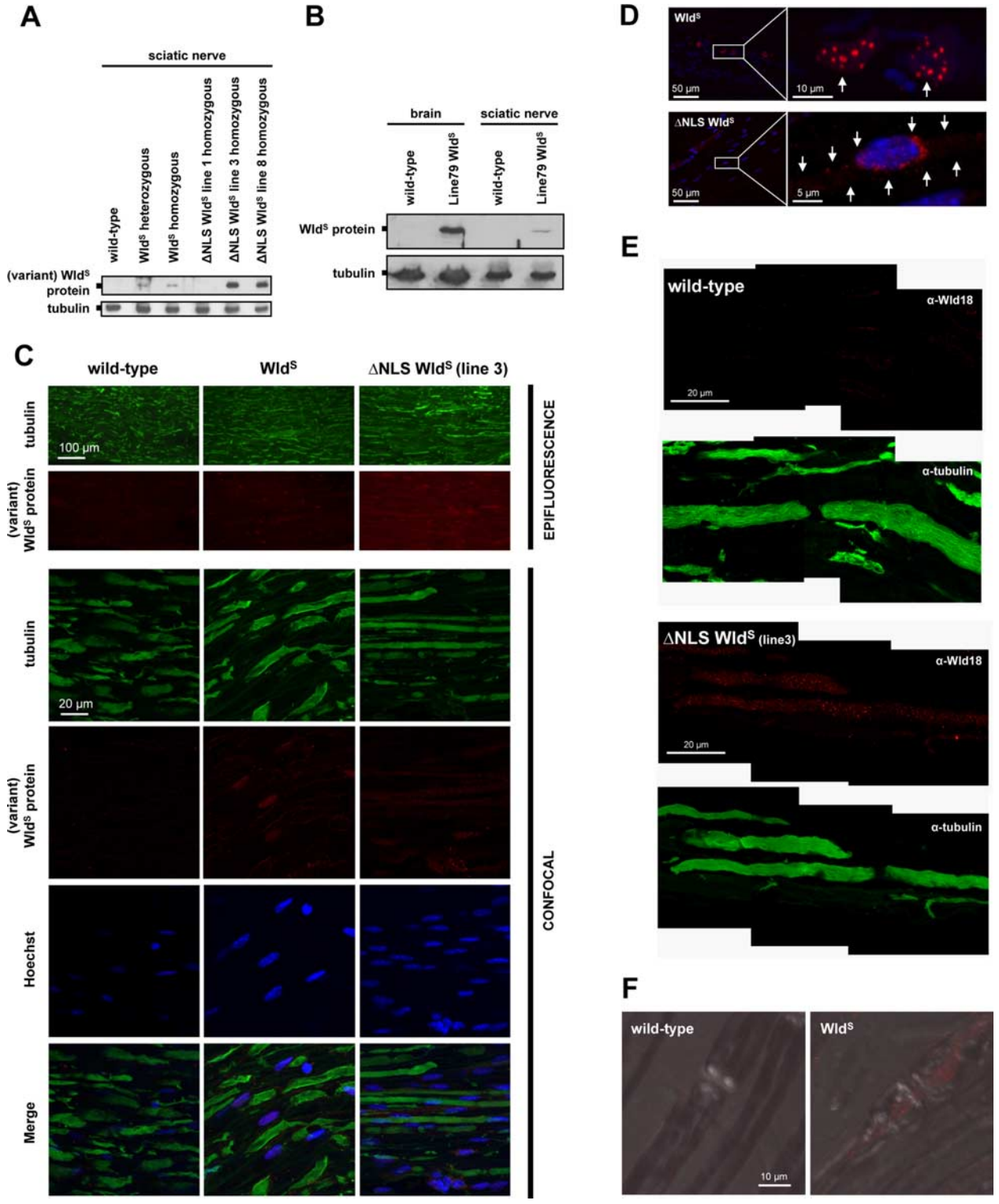

Figure 6. Detection of Wld^S and variant ΔNLS Wld^S proteins in nerves *in vivo*. ***A***, Western blot showing presence of variant Wld^S proteins in sciatic nerve extracts from both spontaneous Wld^S mice and ΔNLS Wld^S transgenics. Note markedly higher levels of variant Wld^S protein in extracts from ΔNLS Wld^S lines 3 and 8 compared with Wld^S (heterozygous and homozygous). ***B***, Western blot showing presence of Wld^S protein in sciatic nerve extracts from transgenic Wld^S rat (line 79, homozygous). For comparison, detection of Wld^S in similar total protein amount from brain homogenate from the same rat is also shown. ***C***, Fluorescence immunostaining on wild-type, Wld^S (homozygous), and ΔNLS Wld^S (line 3, homozygous) longitudinal sciatic nerve sections using tubulin (green) and Wld18 (red) antibodies. Conventional epifluorescence microscopy (rows 1 and 2) demonstrates more intense Wld18 labeling in sciatic nerve from ΔNLS Wld^S mouse than from Wld^S. Higher-resolution confocal images (rows 3–6) from the same sections show variant Wld^S protein signals in glial cells whose nuclei were counterstained with Hoechst 33258 (blue). Note more prominent Wld18 staining in sample from ΔNLS Wld^S sciatic nerve. ***D***, Confocal images showing induction of variant Wld^S expression (red) in glial cells 6 h after sciatic nerve injury located distally from the lesion site. Note nuclear Wld^S foci in activated glial cells (arrows, upper row) from native Wld^S mutant, whereas induced ΔNLS Wld^S protein expression shows a more cytoplasmic staining pattern demarcating the cell body (arrows, lower row). Blue, Hoechst 33258 counterstain. ***E***, High-power confocal composite (*z*-series projection) shows presence and homogenous distribution of variant Wld^S protein (red) in the nodal and internodal axoplasm of ΔNLS Wld^S sciatic nerve (line 3) which is counterstained with tubulin (green). Note the fine granular staining pattern of Wld18 antibody within the axoplasm. Variant Wld^S protein immunoreactivity is absent from wild-type sciatic axons. ***F***, Confocal images (*z*-series projection + DIC merge) showing localization of Wld^S protein (red) in nodal and perinodal axoplasm of native Wld^S axon in contrast to wild-type fiber where Wld^S signal is absent (Wld18 antibody plus Alexa568-tyramide signal amplification).

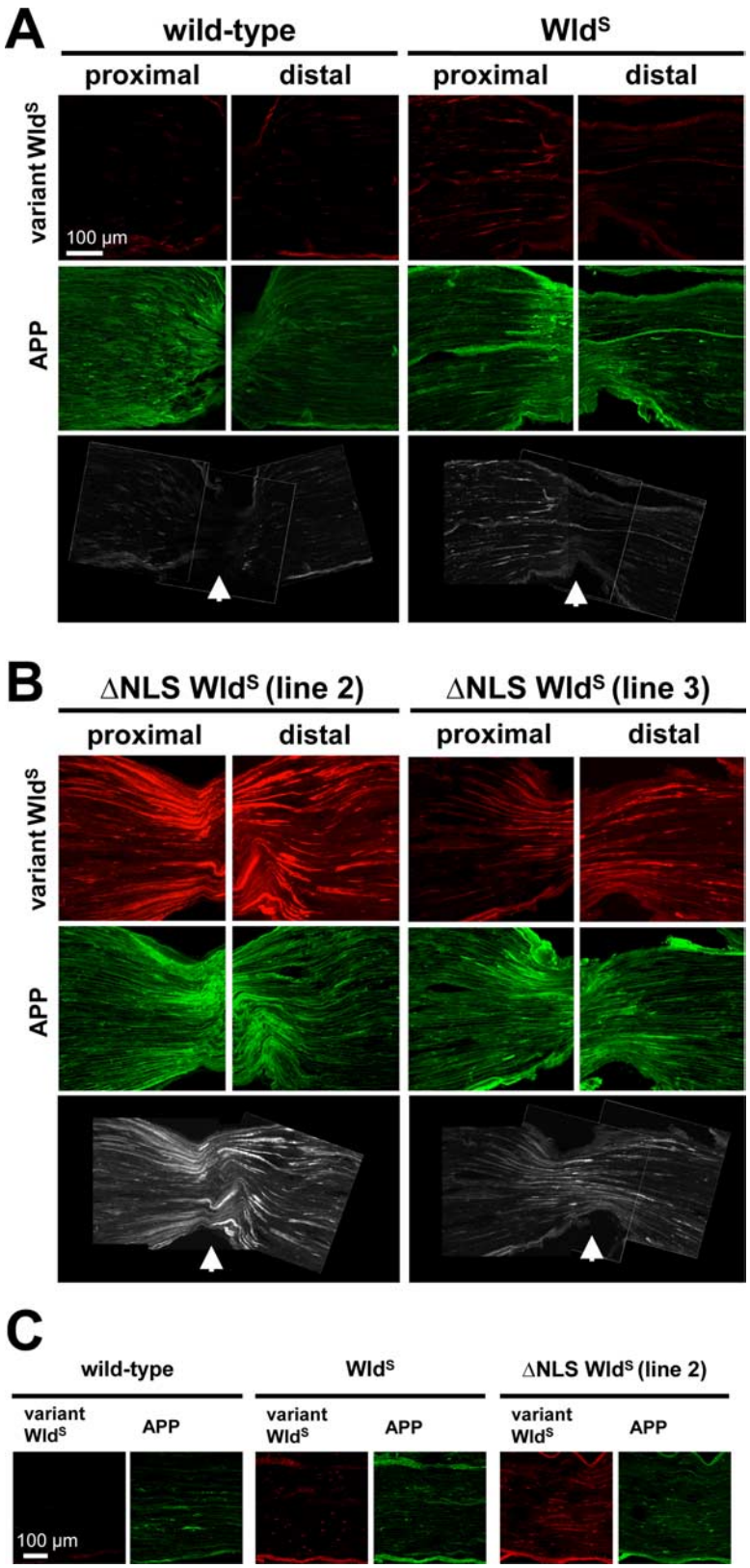

Figure 7. Accumulation of variant Wld^S at the site of nerve constriction. ***A***, ***B***, Fluorescence double immunostaining on longitudinal sciatic nerve sections proximal and distal to crush site (6 h p.o.) using Wld18 (red) and APP (green) antibodies. Confocal projections demonstrate no Wld18 signal in wild type (***A***, left), weak Wld18 signal in nerve portions from native Wld^S (***A***, right) and substantial accumulation of variant Wld^S protein signal proximal and distal to the crush site in ΔNLS Wld^S sciatic nerves (***B***, lines 2 and 3 homozygous). APP immunosignal is enriched in proximal portions close to the crush site in all samples at this time point. Confocal survey composites in bottom panels show the position of surgical nerve constriction (arrows) in relation to adjacent nerve segments. ***C***, Control double immunostaining on unlesioned longitudinal sciatic nerve segments from wild-type, native Wld^S, and ΔNLS Wld^S mice for comparison with ***A*** and ***B***.

sion is sufficient for Wld^S neuroprotection and delay of Wallerian degeneration can be observed *in vitro* in the virtual absence of glia (Glass et al., 1993; MacDonald et al., 2006; Conforti et al., 2007). Using this method and high-power confocal imaging we also observed weak axonal staining in ΔNLS Wld^S but not in native Wld^S and wild-type sciatic nerve sections (Fig. 6*E*; supplemental Fig. 5, available at www.jneurosci.org as supplemental material; and not shown). Axoplasmic ΔNLS Wld^S protein was distributed throughout nodes and internodes of individual sciatic nerve axons in a fine granular staining pattern (Fig. 6*E*). To test whether variant Wld^S protein remains detectable after axotomy we conducted Western blotting and immunofluorescence on distal sciatic nerve stumps from ΔNLS Wld^S transgenic mice 1 week following lesion (supplemental Fig. 6, available at www.jneurosci.org as supplemental material). The protein was still present at this time, consistent with a direct axonal role, and no changes in staining pattern could be observed (supplemental Fig. 6*B*, available at www.jneurosci.org as supplemental material).

The presence of variant Wld^S protein in the axoplasm raises the possibility that it could be transported anterogradely and/or retrogradely. To test this and to further enhance the signal, we performed focal sciatic nerve crush injury and immunostained cryosections with Wld18 as above and additionally with APP antibody (Fig. 7). As previously shown (Cavalli et al., 2005), sciatic nerve crush caused a focal block of axonal transport, and APP accumulated primarily at the proximal side close to the injury point 6 h following lesion in mice of each genotype (Fig. 7*A*,*B*). A small increase in Wld^S signal was seen at crush sites of native Wld^S nerves, although this may reflect glial signal induced by the lesion (see above). An altogether more striking and clearly axonal signal was evident on both sides of the crush in ΔNLS Wld^S axons. This suggests that at least the variant ΔNLS Wld^S protein is transported both anterogradely and retrogradely in fast axonal transport, to account for this build up within 6 h, although more direct evidence will be needed to confirm this.

To assess whether presence of Wld^S can be demonstrated in native Wld^S axons by increasing detection sensitivity we exploited catalyzed reporter deposition (CARD) of tyramide derivatives (Van Heusden et al., 1997). Similar to the results in nerves from ΔNLS Wld^S transgenics, this method revealed also axoplasmic Wld^S in granular staining pattern at native

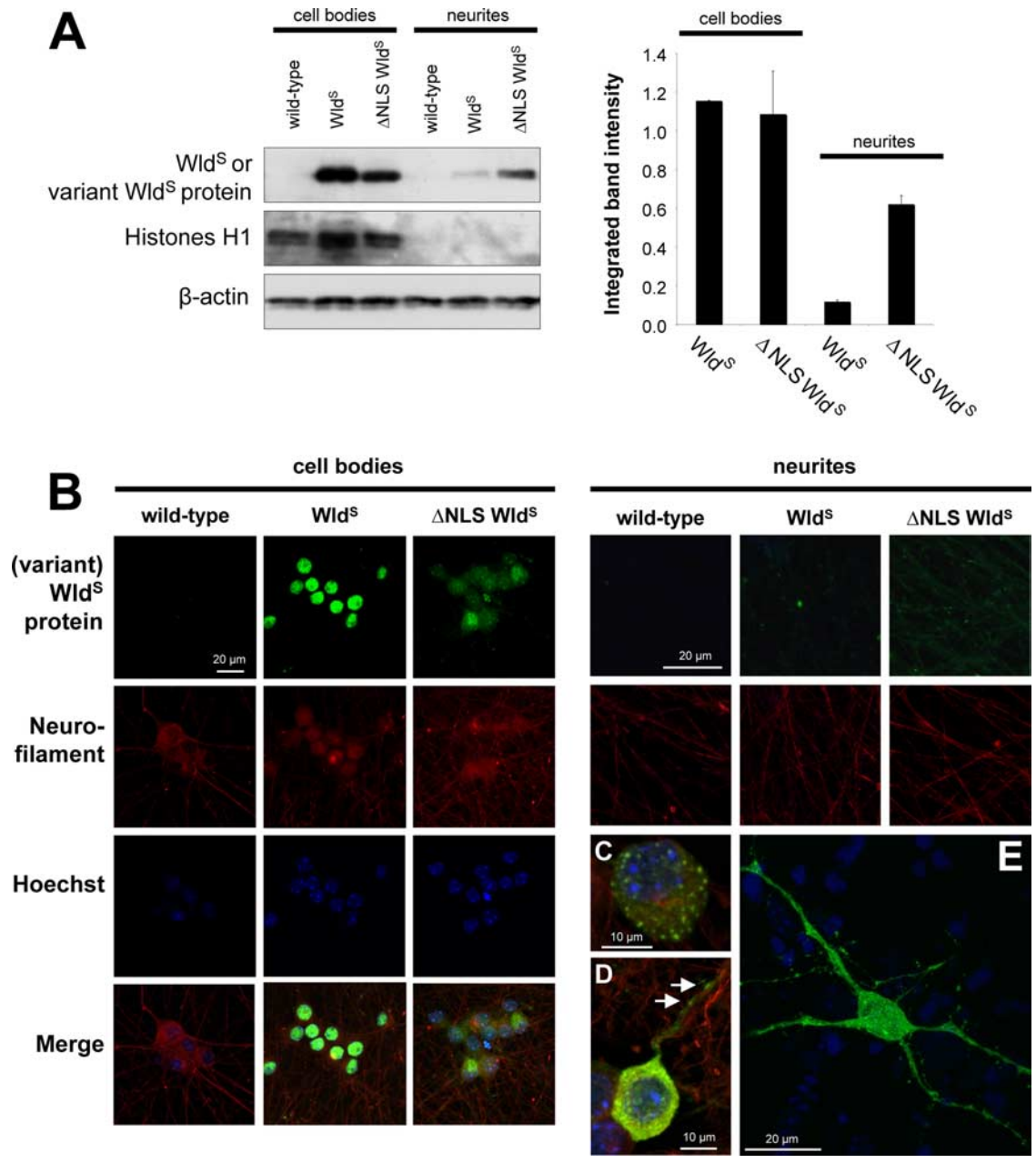

Figure 8. Visualization of Wld^S and variant ΔNLS Wld^S distribution in primary neuronal culture. ***A***, Left, Western blot from SCG cell body/proximal neurite ("cell bodies") and distal neurite fractions ("neurites") showing Wld^S and variant Wld^S in neurites. Note the reduced level of variant ΔNLS Wld^S in cell bodies and significantly increased levels in neurites. To rule out nuclear contamination derived from glial and other cells in neurite fractions, Western blots were probed with the nuclear marker Histones H1. Right, Densitometric quantification of variant Wld^S protein (normalized to β-actin). Data from two independent experiments are presented as mean ± SD. ***B***, Left, Confocal images showing cell bodies (and proximal neurites) from dissociated SCG preparations labeled with Wld18 antibody (green; Alexa488-tyramide signal amplification), neurofilament antibody (red) and DAPI (blue). Note cytoplasmic redistribution of the ΔNLS Wld^S protein variant relative to Wld^S. Right, Higher magnification confocal images demonstrating variant Wld^S in SCG neurites (green; Alexa488-tyramide signal amplification). ***C***, ***D***, High-power confocal projections demonstrating peri-nuclear variant Wld^S foci (green) in SCG preparation from ΔNLS Wld^S transgenic mouse (***C***) and occasional foci in proximal neurites (***D***, arrows). ***E***, Confocal projection showing transfected hippocampal neuron expressing ΔNLS Wld^S-EGFP fusion protein. Note cytoplasmic ΔNLS Wld^S-EGFP foci in cell body and neurites.

Wld^S nodes and internodes (Fig. 6*F*), with lack of signal in wild type indicating specificity.

For further corroboration we then studied axonal Wld^S in superior cervical ganglion (SCG) explants (Fig. 8*A*) to exclude glia, reduce the dilution of Wld^S into the large axonal volume and to isolate neurites in the virtual absence of cell bodies. A robust Wld^S phenotype was present in explants from both Wld^S and ΔNLS Wld^S mice (data not shown). Neuritic extracts from Wld^S and ΔNLS Wld^S explants showed a clear Western blotting signal that was markedly stronger in the latter ($N = 4$ experiments) (Fig. 8*A*). CARD immunostaining confirmed protein redistribution showing decreased nuclear staining and distinct labeling of neurites in ΔNLS Wld^S SCGs and DRGs (Fig. 8*B* and data not shown). Interestingly, cell bodies and occasionally axons of many neurons showed discrete variant Wld^S foci of varying size (Figs. 8*C*,*D*, 9*B*,*D*). Longer tyramide deposition reaction times revealed cytoplasmic foci also for native Wld^S but not for wild-type controls. Variant Wld^S foci were also present in hippocampal cultures transfected with a ΔNLS Wld^S construct fused to EGFP (Fig. 8*E*). However, such foci were never observed *in situ* in brain

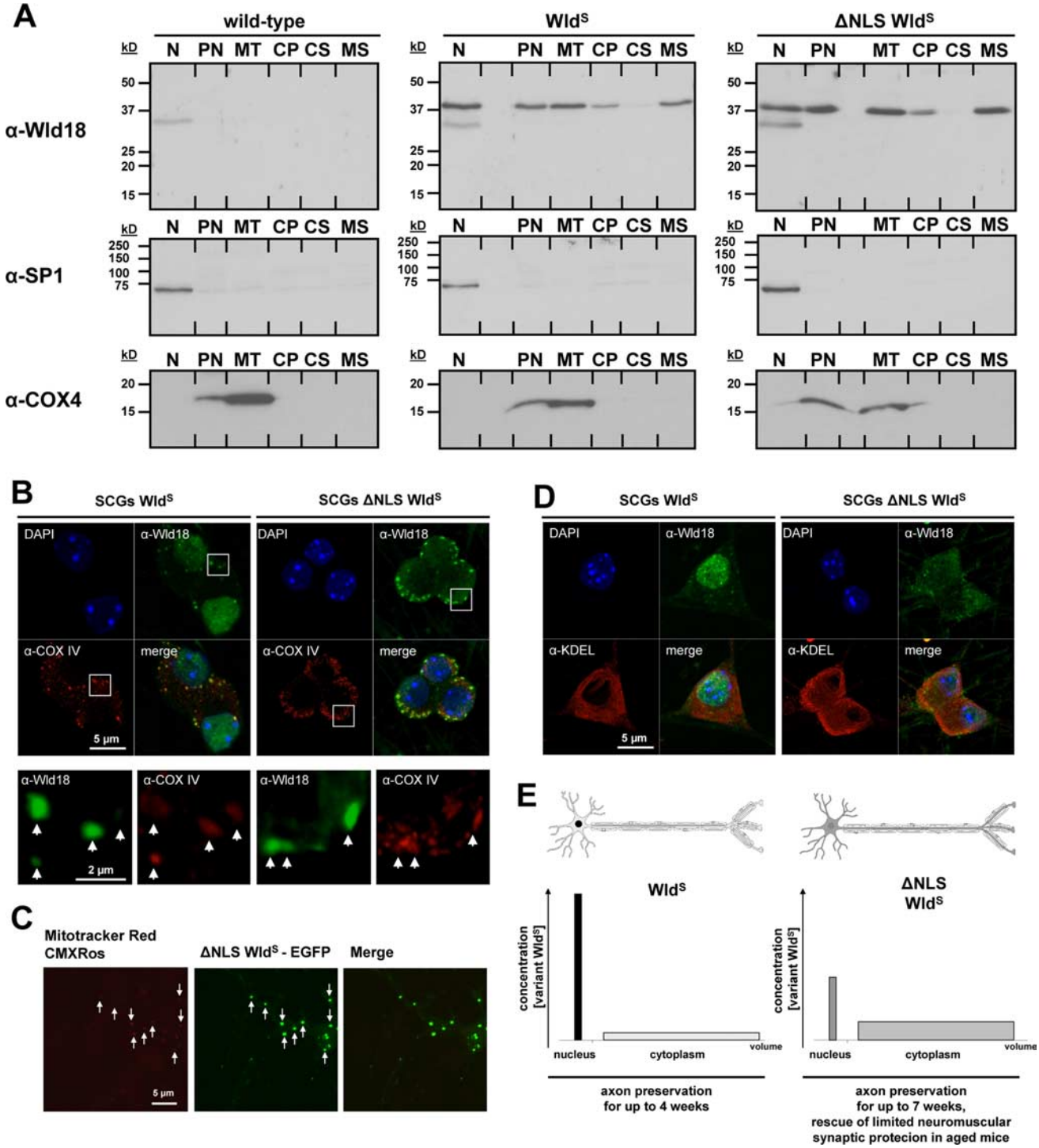

Figure 9. Wld^S and variant ΔNLS Wld^S proteins associate with mitochondria and microsomes. ***A***, Western blot of Wld^S variants in subcellular fractions from mouse brain: N, nuclear; PN, postnuclear; MT, mitochondrial; CP, cytoplasmic; CS, cytosolic; MS, microsomal. Nuclear SP-1 and mitochondrial marker COX-IV were used to assess the fractionation. ***B***, Confocal images of SCG neurons labeled with Wld18 (green; Alexa488-tyramide signal amplification) and COXIV (red) antibodies. White squares represent higher magnification insets shown in lower panel. Arrows indicate partial colocalization of Wld18 and COXIV. ***C***, Confocal live cell imaging of hippocampal neuron expressing variant ΔNLS Wld^S fused to EGFP (green). The preparation was labeled with Mitotracker Red CMXRos (red). Arrows indicate partial colocalization of ΔNLS Wld^S-EGFP and mitochondria. ***D***, Confocal images of SCG neurons labeled with Wld18 (green; Alexa488-tyramide signal amplification) and KDEL (red; as ER marker) antibodies. Note many extranuclear variant Wld^S foci overlap with the KDEL endoplasmic reticulum marker signals. ***E***, Schematic illustration summarizing non-nuclear-mediated delay of Wallerian degeneration: altered ratio of nuclear versus cytoplasmic Wld^S content results in more robust neuroprotection in ΔNLS Wld^S transgenics. The graphs demonstrate distribution of Wld^S (left) with high concentration in the smaller nuclear compartment and low concentration in the much larger cytoplasmic compartment. In contrast, ΔNLS Wld^S (right) is altered in favor of the large cytoplasmic compartment resulting in easier detectability and in more robust axon and synapse protection.

or spinal cord neurons from ΔNLS Wld^S transgenics or spontaneous Wld^S mice, presumably due to lower concentrations of the variant Wld^S proteins *in vivo* and/or antigen masking through fixation and embedding procedures.

Together, these results suggest presence of extranuclear Wld^S in axons with higher axoplasmic levels in ΔNLS Wld^S transgenic mice and the possibility of axonal transport of Wld^S variants.

Wld^S and variant ΔNLS Wld^S proteins associate with mitochondria and intracellular membranes

Finally, we studied the association of Wld^S and variant Wld^S with organelles in subcellular fractionation of brain tissue and in cell culture. Wld^S and variant Wld^S were detectable both in enriched mitochondrial (MT) and intracellular membrane (microsome) fractions (MS) but absent in wild type (Fig. 9*A*). Similar data were obtained from transgenic Wld^S rats (data not shown). In CARD analysis, ~85% of extranuclear native or variant Wld^S foci partially colocalized with mitochondria, although many mitochondria were not colocalized (Fig. 9*B*). Again, wild-type controls lacked these foci (supplemental Fig. 7*A*, available at www.jneurosci.org as supplemental material). In transfected hippocampal primary cultured neurons and PC12 cells, ~90% and 60% of ΔNLS Wld^S-EGFP foci partially colocalized with Mitotracker Red CMXRos (Fig. 9*C*) or DsRed2-Mito, respectively, and linear fluorescence intensity profiles confirmed partial colocalization (supplemental Fig. 7*B*, available at www.jneurosci.org as supplemental material). Many other Wld^S foci were adjacent to mitochondria, but conversely most mitochondria in PC12 cells were not detectably associated with Wld^S, suggesting association with a subset of mitochondria. Additionally, we observed partial association between extranuclear Wld^S variants and the endoplasmic reticulum marker KDEL (anti-MAC256 antibody) in SCG neurons (Fig. 9*D*). Analysis of SCG neurons costained with LAMP-2 antibodies (anti-ABL-93) did not indicate any association with lysosomes (data not shown).

Discussion

These data show that the effectiveness of Wld^S mediated neuroprotection *in vivo* is highly dependent on non-nuclear levels of the mutant protein, indicating a cytoplasmic or even direct axonal role for Wld^S (Fig. 9*E*). We detect native Wld^S protein outside the nucleus and in axons for the first time *in vivo* and report novel subcellular localization to mitochondria and microsome fractions. In addition to these insights into the protective mechanism, the increased efficacy will improve assessment of which neurodegenerative disorders involve Wallerian-like degeneration and points to more optimal therapeutic strategies based around Wld^S.

Wld^S protection has been shown to be strongly dose-dependent by the weaker phenotype of C57BL/Wld^S heterozygotes in both injury and disease (Perry et al., 1992; Mack et al., 2001; Samsam et al., 2003; Mi et al., 2005) and by strong correlation between expression level and phenotype strength in Wld^S transgenic lines (Mack et al., 2001; Adalbert et al., 2005). Surprisingly, we found that reduced nuclear targeting of Wld^S without altering total expression level strengthens the protective phenotype, rather than weakening it as a nuclear action would predict. The maximum axon survival following sciatic nerve transection was extended from 4 to 7 weeks and very weakly expressing lines were able to confer a robust Wld^S phenotype. Intriguingly, the increased efficacy of the ΔNLS Wld^S variant is particularly striking at motor nerve terminals from older mice, where native Wld^S is far less effective than in the axon trunk (Mack et al., 2001; Gillingwater et al., 2002).

The reason for the substantial weakening of functional NMJ protection in older Wld^S mice is unknown but appears not to involve any decrease in Wld^S expression (Gillingwater et al., 2002). In contrast to spontaneous and transgenic Wld^S mice, ΔNLS Wld^S dramatically retained its ability to preserve neuromuscular synapses in older mice as well as increasing the maximum survival of axotomized NMJs in younger mice. We previously reported enhanced NMJ protection after sciatic nerve lesion in transgenic Wld^S rats and speculated that the longer distal axon stump relative to mice might be responsible (Adalbert et al., 2005). In Wld^S mice lengthening the distal stump delays degeneration of NMJs by 1–2 d/cm (Ribchester et al., 1995). One model to explain this could be that Wld^S neuromuscular synapses require continuous supply of a neuroprotective factor for their survival. We hypothesize now that this putative factor could be axonally transported Wld^S itself. As rate of axonal transport declines with age (Cross et al., 2008) the weakening of protective phenotype in old Wld^S mutants could be explained with this model. Axonal Wld^S protein may fall below an efficacy threshold for synaptic maintenance as mice age. This might not occur in old ΔNLS Wld^S transgenics due to the overall higher variant Wld^S levels in axons (as shown for sciatic nerves). Although we provide preliminary data suggesting fast axonal transport of at least variant ΔNLS Wld^S protein in sciatic nerve, further experiments addressing the relative levels of Wld^S variants being transported and at synapses will be needed to test this hypothesis.

Several hypotheses for Wld^S action now need to be reexamined to ask how each fits with these new data. For instance, mechanisms involving action of Wld^S exclusively in nuclei now appear unlikely, although we cannot rule out a simultaneous action in both cytoplasm and nuclei. Reports of gene expression changes in Wld^S mice (Gillingwater et al., 2006; Simonin et al., 2007b) may be less linked to the high nuclear Wld^S concentration than expected and feedback mechanisms from cytoplasmic Wld^S could be one other explanation for the gene expression data. Previous data based on strong lentiviral overexpression of Nmnat1 in DRG neurons suggested efficacy was independent of subcellular targeting (Sasaki et al., 2006) although it is not clear whether this reflects the axon protection mechanism *in vivo* (Conforti et al., 2007). Altered gene regulation driven by the NAD^+ dependent deacetylase sirtuin 1 (Sirt1), a nuclear enzyme (Araki et al., 2004) now appears unlikely and a role for Sirt1 was already hard to reconcile with axon protection in Sirt1 null neurons (Wang et al., 2005) (M. Avery, S. Sheehan, K. Kerr, J. Wang, and M. Freeman, unpublished work). A non-nuclear site of action for Wld^S now casts further doubt on a mechanism involving nuclear Sirt1. Instead, our data are consistent with local axonal protection mechanisms, proposed previously based on *in vitro* data (Wang et al., 2005). Although we demonstrate localization of Wld^S variants to axons *in vivo* additional targeting studies will be needed to address whether the critical site is within the axon itself or in the cell body cytoplasm.

Once Wld^S is targeted to a specific non-nuclear site, the associated, essential Nmnat activity (Araki et al., 2004) is likely to produce a high local NAD^+ concentration. The existence of multiple pathways for NAD^+ catabolism (Berger et al., 2004) may help explain why this increase has not been detected more generally (Mack et al., 2001; Araki et al., 2004), as once generated NAD^+ will be rapidly and locally degraded. While it persists, however, this tightly localized NAD^+ may be used to influence downstream calcium signaling (Berger et al., 2004), bioenergetics (Di Lisa and Ziegler, 2001; Wang et al., 2005), protein modification (Berger et al., 2004) or other functions near its site of production (Berger et al., 2007). The presence of Wld^S in the mitochondrial fraction and the partial colocalization with a subset of mitochondria *in vitro*, as observed for other proteins (Kang et al., 2008), are consistent with a bioenergetics or signaling role, as mitochondria require NAD^+ to synthesize ATP and to regulate signaling pathways necessary for cell viability (Di Lisa and Ziegler, 2001; Yang et al., 2007a). However, although Wld^S axons

maintain both NAD^+ and ATP levels after axon lesion better than wild type (Ikegami and Koike, 2003; Wang et al., 2005), a causal role for bioenergetic metabolism in Wld^S mechanism is unproven. A recent *in vitro* study suggests an alternative mechanism based on Nmnat blocking production of reactive oxygen species (ROS) from mitochondria (Press and Milbrandt, 2008).

Other data regarding the molecular mechanism of Wld^S mediated axon protection suggest involvement of valosin-containing protein (VCP) that binds the N-terminal 16 aa of Wld^S through a VCP binding motif (Laser et al., 2006). This region is necessary but not sufficient for axon protection in mice (Conforti et al., 2007) (Conforti, Wilbrey, Morreale, Janeckova, Beirowski, Adalbert, Mazzola, Di Stefano, Hartley, Babetto, Smith, Gilley, Billington, Genazzani, Ribchester, Magni, and Coleman, unpublished work) and is necessary for full strength phenotype in *Drosophila* (Avery, Sheehan, Kerr, Wang, and Freeman, unpublished work). Another recent study showed that VCP binding is required for Wld^S to localize to discrete subnuclear foci (Wilbrey et al., 2008). These nuclear foci were not required for the protective phenotype, but may reflect a more general fine localization mechanism that is relevant also to Wld^S in other compartments. VCP is a ubiquitous cellular protein with high concentrations in the neuronal cytoplasm (Wang et al., 2004; Laser et al., 2006). The high cytoplasmic VCP content is likely to drive Wld^S-VCP binding, particularly at sites where VCP is most abundant. One such site is the endoplasmic reticulum (ER), where protein binding interactions with Hrd1, gp78, and Derlin-1 recruit VCP (Schulze et al., 2005). The presence of Wld^S in microsome fraction where detection of VCP has been also reported (Madeo et al., 1998) is consistent with an ER localization, although the incomplete colocalization with ER suggests either that Wld^S is restricted to ER subdomains and/or that it is restricted to a different microsome component.

ΔNLS Wld^S transgenic mice should considerably enhance axon and synapse protection also in neurodegeneration models. Thus far, Wld^S showed significant axon protection in several disorders such as progressive motor neuronopathy (*pmn*) (Ferri et al., 2003), peripheral neuropathy (Samsam et al., 2003) and chronic or induced glaucoma (Howell et al., 2007; Beirowski et al., 2009), but was less effective in others, most notably in mouse models of familial ALS (Vande Velde et al., 2004; Fischer et al., 2005). The modest or even undetectable neuroprotective effect in Wld^S/SOD1 mutants was unexpected, given that these mice have axonal transport deficiencies (Vande Velde et al., 2004) and that axonal transport impairment appears to underlie the *pmn* phenotype. In fact, Wld^S does confer significant protection of motor nerve terminals in SOD1 (G93A) mutant mice at least up to 80 d of age but not thereafter (Fischer et al., 2005), suggesting that the age-dependent weakening of synaptic protection in Wld^S mice could explain its inability to alter the SOD1 phenotype strongly. It will be important to test now whether the ΔNLS Wld^S variant could overcome this limit of neuroprotection.

We conclude that Wld^S is able to exert extensive neuroprotective effects on axons and synapses through a non-nuclear action, indicating an urgent need to address the roles of NAD^+ synthesis and other Wld^S functions such as VCP binding in these locations. We show that the efficacy of Wld^S can be increased by appropriate subcellular targeting, so future studies can now address whether the critical location is axonal or cytoplasmic, whether mitochondria or one of the microsome compartments are involved, and whether the enhanced protection offered by the ΔNLS Wld^S variant can be developed into more effective therapy for axonopathies.

References

Adalbert R, Gillingwater TH, Haley JE, Bridge K, Beirowski B, Berek L, Wagner D, Grumme D, Thomson D, Celik A, Addicks K, Ribchester RR, Coleman MP (2005) A rat model of slow Wallerian degeneration (WldS) with improved preservation of neuromuscular synapses. Eur J Neurosci 21:271–277.

Araki T, Sasaki Y, Milbrandt J (2004) Increased nuclear NAD biosynthesis and SIRT1 activation prevent axonal degeneration. Science 305:1010–1013.

Barry JA, Ribchester RR (1995) Persistent polyneuronal innervation in partially denervated rat muscle after reinnervation and recovery from prolonged nerve conduction block. J Neurosci 15:6327–6339.

Beirowski B, Berek L, Adalbert R, Wagner D, Grumme DS, Addicks K, Ribchester RR, Coleman MP (2004) Quantitative and qualitative analysis of Wallerian degeneration using restricted axonal labelling in YFP-H mice. J Neurosci Methods 134:23–35.

Beirowski B, Adalbert R, Wagner D, Grumme DS, Addicks K, Ribchester RR, Coleman MP (2005) The progressive nature of Wallerian degeneration in wild-type and slow Wallerian degeneration (WldS) nerves. BMC Neurosci 28:1166–1179.

Beirowski B, Babetto E, Coleman PM, Martin RM (2009) The WldS gene delays axonal but not somatic degeneration in a rat glaucoma model. Eur J Neurosci, in press.

Berger F, Ramírez-Hernández MH, Ziegler M (2004) The new life of a centenarian: signalling functions of NAD(P). Trends Biochem Sci 29:111–118.

Berger F, Lau C, Ziegler M (2007) Regulation of poly(ADP-ribose) polymerase 1 activity by the phosphorylation state of the nuclear NAD biosynthetic enzyme NMN adenylyl transferase 1. Proc Natl Acad Sci U S A 104:3765–3770.

Betz WJ, Mao F, Bewick GS (1992) Activity-dependent fluorescent staining and destaining of living vertebrate motor nerve terminals. J Neurosci 12:363–375.

Cavalli V, Kujala P, Klumperman J, Goldstein LS (2005) Sunday Driver links axonal transport to damage signaling. J Cell Biol 168:775–787.

Coleman M (2005) Axon degeneration mechanisms: commonality amid diversity. Nat Rev Neurosci 6:889–898.

Coleman MP, Conforti L, Buckmaster EA, Tarlton A, Ewing RM, Brown MC, Lyon MF, Perry VH (1998) An 85-kb tandem triplication in the slow Wallerian degeneration (Wlds) mouse. Proc Natl Acad Sci U S A 95:9985–9990.

Conforti L, Tarlton A, Mack TG, Mi W, Buckmaster EA, Wagner D, Perry VH, Coleman MP (2000) A Ufd2/D4Cole1e chimeric protein and overexpression of rbp7 in the slow Wallerian degeneration (WldS) mouse. Proc Natl Acad Sci U S A 97:11377–11382.

Conforti L, Fang G, Beirowski B, Wang MS, Sorci L, Asress S, Adalbert R, Silva A, Bridge K, Huang XP, Magni G, Glass JD, Coleman MP (2007) NAD(+) and axon degeneration revisited: Nmnat1 cannot substitute for Wld(S) to delay Wallerian degeneration. Cell Death Differ 14:116–127.

Cross DJ, Flexman JA, Anzai Y, Maravilla KR, Minoshima S (2008) Age-related decrease in axonal transport measured by MR imaging in vivo. Neuroimage 39:915–926.

Di Lisa F, Ziegler M (2001) Pathophysiological relevance of mitochondria in NAD(+) metabolism. FEBS Lett 492:4–8.

Fainzilber M, Twiss JL (2006) Tracking in the Wlds—the hunting of the SIRT and the luring of the Draper. Neuron 50:819–821.

Fang C, Bernardes-Silva M, Coleman MP, Perry VH (2005) The cellular distribution of the Wld s chimeric protein and its constituent proteins in the CNS. Neuroscience 135:1107–1118.

Feng G, Mellor RH, Bernstein M, Keller-Peck C, Nguyen QT, Wallace M, Nerbonne JM, Lichtman JW, Sanes JR (2000) Imaging neuronal subsets in transgenic mice expressing multiple spectral variants of GFP. Neuron 28:41–51.

Ferri A, Sanes JR, Coleman MP, Cunningham JM, Kato AC (2003) Inhibiting axon degeneration and synapse loss attenuates apoptosis and disease progression in a mouse model of motoneuron disease. Curr Biol 13:669–673.

Fischer LR, Culver DG, Davis AA, Tennant P, Wang M, Coleman M, Asress S, Adalbert R, Alexander GM, Glass JD (2005) The Wld(S) gene modestly prolongs survival in the SOD1(G93A) fALS mouse. Neurobiol Dis 19:293–300.

Gillingwater TH, Thomson D, Mack TG, Soffin EM, Mattison RJ, Coleman

MP, Ribchester RR (2002) Age-dependent synapse withdrawal at axotomised neuromuscular junctions in Wld(s) mutant and Ube4b/Nmnat transgenic mice. J Physiol 543:739–755.

Gillingwater TH, Wishart TM, Chen PE, Haley JE, Robertson K, MacDonald SH, Middleton S, Wawrowski K, Shipston MJ, Melmed S, Wyllie DJ, Skehel PA, Coleman MP, Ribchester RR (2006) The neuroprotective WldS gene regulates expression of PTTG1 and erythroid differentiation regulator 1-like gene in mice and human cells. Hum Mol Genet 15:625–635.

Glass JD, Brushart TM, George EB, Griffin JW (1993) Prolonged survival of transected nerve fibres in C57BL/Ola mice is an intrinsic characteristic of the axon. J Neurocytol 22:311–321.

Hamilton MH, Tcherepanova I, Huibregtse JM, McDonnell DP (2001) Nuclear import/export of hRPF1/Nedd4 regulates the ubiquitin-dependent degradation of its nuclear substrates. J Biol Chem 276:26324–26331.

Hoopfer ED, McLaughlin T, Watts RJ, Schuldiner O, O'Leary DD, Luo L (2006) Wlds protection distinguishes axon degeneration following injury from naturally occurring developmental pruning. Neuron 50:883–895.

Howell GR, Libby RT, Jakobs TC, Smith RS, Phalan FC, Barter JW, Barbay JM, Marchant JK, Mahesh N, Porciatti V, Whitmore AV, Masland RH, John SW (2007) Axons of retinal ganglion cells are insulted in the optic nerve early in DBA/2J glaucoma. J Cell Biol 179:1523–1537.

Ikegami K, Koike T (2003) Non-apoptotic neurite degeneration in apoptotic neuronal death: pivotal role of mitochondrial function in neurites. Neuroscience 122:617–626.

Kang JS, Tian JH, Pan PY, Zald P, Li C, Deng C, Sheng ZH (2008) Docking of axonal mitochondria by syntaphilin controls their mobility and affects short-term facilitation. Cell 132:137–148.

Kay AR, Alfonso A, Alford S, Cline HT, Holgado AM, Sakmann B, Snitsarev VA, Stricker TP, Takahashi M, Wu LG (1999) Imaging synaptic activity in intact brain and slices with FM1–43 in *C. elegans*, lamprey, and rat. Neuron 24:809–817.

Laser H, Conforti L, Morreale G, Mack TG, Heyer M, Haley JE, Wishart TM, Beirowski B, Walker SA, Haase G, Celik A, Adalbert R, Wagner D, Grumme D, Ribchester RR, Plomann M, Coleman MP (2006) The slow Wallerian degeneration protein, WldS, binds directly to VCP/p97 and partially redistributes it within the nucleus. Mol Biol Cell 17:1075–1084.

Liu J, Lillo C, Jonsson PA, Vande Velde C, Ward CM, Miller TM, Subramaniam JR, Rothstein JD, Marklund S, Andersen PM, Brännström T, Gredal O, Wong PC, Williams DS, Cleveland DW (2004) Toxicity of familial ALS-linked SOD1 mutants from selective recruitment to spinal mitochondria. Neuron 43:5–17.

MacDonald JM, Beach MG, Porpiglia E, Sheehan AE, Watts RJ, Freeman MR (2006) The *Drosophila* cell corpse engulfment receptor Draper mediates glial clearance of severed axons. Neuron 50:869–881.

Mack TG, Reiner M, Beirowski B, Mi W, Emanuelli M, Wagner D, Thomson D, Gillingwater T, Court F, Conforti L, Fernando FS, Tarlton A, Andressen C, Addicks K, Magni G, Ribchester RR, Perry VH, Coleman MP (2001) Wallerian degeneration of injured axons and synapses is delayed by a Ube4b/Nmnat chimeric gene. Nat Neurosci 4:1199–1206.

Madeo F, Schlauer J, Zischka H, Mecke D, Fröhlich KU (1998) Tyrosine phosphorylation regulates cell cycle-dependent nuclear localization of Cdc48p. Mol Biol Cell 9:131–141.

Mi W, Beirowski B, Gillingwater TH, Adalbert R, Wagner D, Grumme D, Osaka H, Conforti L, Arnhold S, Addicks K, Wada K, Ribchester RR, Coleman MP (2005) The slow Wallerian degeneration gene, WldS, inhibits axonal spheroid pathology in gracile axonal dystrophy mice. Brain 128:405–416.

Namimatsu S, Ghazizadeh M, Sugisaki Y (2005) Reversing the effects of formalin fixation with citraconic anhydride and heat: a universal antigen retrieval method. J Histochem Cytochem 53:3–11.

Okado-Matsumoto A, Fridovich I (2001) Subcellular distribution of superoxide dismutases (SOD) in rat liver: Cu,Zn-SOD in mitochondria. J Biol Chem 276:38388–38393.

Perry VH, Lunn ER, Brown MC, Cahusac S, Gordon S (1990) Evidence that the rate of Wallerian degeneration is controlled by a single autosomal dominant gene. Eur J Neurosci 2:408–413.

Perry VH, Brown MC, Tsao JW (1992) The effectiveness of the gene which slows the rate of Wallerian degeneration in C57BL/Ola mice declines with age. Eur J Neurosci 4:1000–1002.

Press C, Milbrandt J (2008) Nmnat delays axonal degeneration caused by mitochondrial and oxidative stress. J Neurosci 28:4861–4871.

Raff MC, Whitmore AV, Finn JT (2002) Axonal self-destruction and neurodegeneration. Science 296:868–871.

Ribchester RR, Tsao JW, Barry JA, Asgari-Jirhandeh N, Perry VH, Brown MC (1995) Persistence of neuromuscular junctions after axotomy in mice with slow Wallerian degeneration (C57BL/WldS). Eur J Neurosci 7:1641–1650.

Sajadi A, Schneider BL, Aebischer P (2004) Wld(s)-mediated protection of dopaminergic fibers in an animal model of Parkinson disease. Curr Biol 14:326–330.

Samsam M, Mi W, Wessig C, Zielasek J, Toyka KV, Coleman MP, Martini R (2003) The Wlds mutation delays robust loss of motor and sensory axons in a genetic model for myelin-related axonopathy. J Neurosci 23:2833–2839.

Sasaki Y, Araki T, Milbrandt J (2006) Stimulation of nicotinamide adenine dinucleotide biosynthetic pathways delays axonal degeneration after axotomy. J Neurosci 26:8484–8491.

Sau D, De Biasi S, Vitellaro-Zuccarello L, Riso P, Guarnieri S, Porrini M, Simeoni S, Crippa V, Onesto E, Palazzolo I, Rusmini P, Bolzoni E, Bendotti C, Poletti A (2007) Mutation of SOD1 in ALS: a gain of a loss of function. Hum Mol Genet 16:1604–1618.

Saxena S, Caroni P (2007) Mechanisms of axon degeneration: from development to disease. Prog Neurobiol 83:174–191.

Schulze A, Standera S, Buerger E, Kikkert M, van Voorden S, Wiertz E, Koning F, Kloetzel PM, Seeger M (2005) The ubiquitin-domain protein HERP forms a complex with components of the endoplasmic reticulum associated degradation pathway. J Mol Biol 354:1021–1027.

Simonin Y, Perrin FE, Kato AC (2007a) Axonal involvement in the Wlds neuroprotective effect: analysis of pure motoneurons in a mouse model protected from motor neuron disease at a pre-symptomatic age. J Neurochem 101:530–542.

Simonin Y, Ferrer-Alcon M, Ferri A, Kato AC (2007b) The neuroprotective effects of the Wld s gene are correlated with proteasome expression rather than apoptosis. Eur J Neurosci 25:2269–2274.

Spencer RL, Kalman BA, Cotter CS, Deak T (2000) Discrimination between changes in glucocorticoid receptor expression and activation in rat brain using Western blot analysis. Brain Res 868:275–286.

Vande Velde C, Garcia ML, Yin X, Trapp BD, Cleveland DW (2004) The neuroprotective factor Wlds does not attenuate mutant SOD1-mediated motor neuron disease. Neuromolecular Med 5:193–203.

Van Heusden J, de Jong P, Ramaekers F, Bruwiere H, Borgers M, Smets G (1997) Fluorescein-labeled tyramide strongly enhances the detection of low bromodeoxyuridine incorporation levels. J Histochem Cytochem 45:315–319.

Waller A (1850) Experiments on the section of glossopharyngeal and hypoglossal nerves of the frog and observations of the alterations produced thereby in the structure of their primitive fibres. Philos Trans R Soc Lond B Biol Sci 140:423–429.

Wang J, Zhai Q, Chen Y, Lin E, Gu W, McBurney MW, He Z (2005) A local mechanism mediates NAD-dependent protection of axon degeneration. J Cell Biol 170:349–355.

Wang Q, Song C, Li CC (2004) Molecular perspectives on p97-VCP: progress in understanding its structure and diverse biological functions. J Struct Biol 146:44–57.

Whitfield J, Neame SJ, Ham J (2004) Methods for culturing primary sympathetic neurons and for determining neuronal viability. Methods Mol Biol 282:157–168.

Wilbrey AL, Haley JE, Wishart TM, Conforti L, Morreale G, Beirowski B, Babetto E, Adalbert R, Gillingwater TH, Smith T, Wyllie DJ, Ribchester RR, Coleman MP (2008) VCP binding influences intracellular distribution of the slow Wallerian degeneration protein, Wld(S). Mol Cell Neurosci 38:325–340.

Yang H, Yang T, Baur JA, Perez E, Matsui T, Carmona JJ, Lamming DW, Souza-Pinto NC, Bohr VA, Rosenzweig A, de Cabo R, Sauve AA, Sinclair DA (2007a) Nutrient-sensitive mitochondrial NAD+ levels dictate cell survival. Cell 130:1095–1107.

Yang Y, Kawataki T, Fukui K, Koike T (2007b) Cellular Zn(2+) chelators cause "dying-back" neurite degeneration associated with energy impairment. J Neurosci Res 85:2844–2855.